Contrib Mineral Petrol (2003) 144: 619–637
DOI 10.1007/s00410-002-0420-3

ORIGINAL PAPER

Leonid V. Danyushevsky · Michael R. Perfit
Stephen M. Eggins · Trevor J. Falloon

Crustal origin for coupled 'ultra-depleted' and 'plagioclase' signatures in MORB olivine-hosted melt inclusions: evidence from the Siqueiros Transform Fault, East Pacific Rise

Received: 31 January 2001 / Accepted: 1 September 2002 / Published online: 29 November 2002

Abstract Geochemical data from melt inclusions in olivine phenocrysts in a picritic basalt from the Siqueiros Transform Fault on the northern East Pacific Rise provide insights into the petrogenesis of mid-ocean ridge basalts (MORB). The fresh lava contains ~10% of olivine phenocrysts ($Fo_{89.3–91.2}$) and rare, small (< 1 mm) plagioclase phenocrysts with subhedral to irregular shapes with a range of compositions ($An_{80–90}$, $An_{57–63}$). Melt inclusions in olivine phenocrysts are glassy, generally rounded in shape and vary in size from a few to ~200 μm. Although most of the inclusions have compositions that are generally consistent with being representative of parental melts for the pillow-rim glasses, several inclusions are clearly different. One inclusion, which contains a euhedral grain of high-Al, low-Ti spinel, has a composition unlike any melt inclusions previously described from primitive phenocrysts in MORB. It has a very high Al_2O_3 (~20 wt%), very low TiO_2 (~0.04 wt%) and Na_2O (~1 wt%) contents, and a very high CaO/Na_2O value (~14). The glass inclusion is strongly depleted in all incompatible elements (La = 0.052 ppm; Yb = 0.34; La/Sm(n) ~0.27), but it has large positive Sr and Eu anomalies (Sr/Sr* ~30; Eu/Eu* ~3) and a negative Zr anomaly. It also has low S (0.015 wt%) and relatively high Cl (180 ppm). We suggest that this unusual composition is a consequence of olivine trapping plagioclase in a hot, strongly plagioclase-undersaturated magma and subsequent reaction between plagioclase and the host olivine producing melt and residual spinel. Two other melt inclusions in a different olivine phenocryst have compositions that are generally intermediate between 'normal' inclusions and the aluminous inclusion, but have even higher CaO and Sr contents. They are also depleted in incompatible elements, but to a lesser degree than the aluminous inclusion, and have smaller Sr and Eu anomalies. Similar inclusions have also been described in high-Fo olivine phenocrysts from Iceland and northern Mid-Atlantic Ridge. We suggest that the compositions of these inclusions represent assimilation of gabbroic material into the hot primitive magma. The localised nature of this assimilation is consistent with it occurring within a crystal mush zone where the porosity is high as primitive magmas pass through earlier formed gabbroic 'cumulates'. In such an environment the contaminants are expected to have quite diverse compositions. Although the interaction of primitive melts with gabbroic material may not affect the compositions of erupted MORB melts on a large scale, this process may be important in some MORB suites and should be accounted for in petrogenetic models. Another important implication is that the observed variability in melt inclusion compositions in primitive MORB phenocrysts need not always to reflect processes occurring in the mantle. In particular, inferences on fractional melting processes based on geochemistry of ultra-depleted melt inclusions may not always be valid.

L.V. Danyushevsky (✉) · T.J. Falloon
School of Earth Sciences and Centre for Ore Deposit Research,
University of Tasmania, G.P.O. Box 252-79,
Hobart, Tasmania 7001, Australia
E-mail: L.Dan@utas.edu.au
Tel.: +61-3-62262469
Fax: +61-3-62232547

M.R. Perfit
Department of Geological Sciences,
Box 112120, University of Florida, Gainesville,
FL 32611-2120, USA

S.M. Eggins
Research School of Earth Sciences;
Australian National University, Canberra,
ACT 0200, Australia

Editorial responsibility: E. Hauri

Introduction

Recent studies of olivine-hosted melt inclusions in primitive mid-ocean-ridge basalts (MORB) have revealed a number of unusual compositions, unlike any

lavas or pillow-rim glasses. In particular, some melt inclusions from Iceland (Sobolev et al. 1994; Gurenko and Chaussidon 1995), the Mid-Atlantic ridge (MAR) near Vema FZ (Sobolev and Shimizu 1993), and Siqueiros FZ, East Pacific Rise (EPR) (Sobolev et al. 1992) have extremely low concentrations of most incompatible elements. Such inclusions are often referred to as ultra-depleted melt (UDM) inclusions (Sobolev and Shimizu 1993). The UDM chemical signature has been suggested to reflect melting processes in the ascending mantle beneath mid-ocean ridges, with UDM inclusions being samples of high-degree (~15%) incremental melt fractions separated from the top of the melting column (e.g. Sobolev and Shimizu 1993).

On the other hand, UDM inclusions from Iceland and Siqueiros FZ, and some melt inclusions from the MAR near the Azores hotspot (Kamenetsky et al. 1998) have large positive Sr anomalies relative to the rare-earth elements (REE) with similar degrees of incompatibility. A similar compositional feature has also been described in olivine-hosted melt inclusions from Hawaii (Sobolev et al. 2000). Major element compositions of the Hawaiian inclusions do not show evidence of plagioclase assimilation and, thus, Sobolev et al. (2000) called their Sr anomalies a 'ghost plagioclase' signature. Sobolev et al. (2000) explained its origin as a result of melting of the recycled oceanic crust present as eclogites in the source of the Hawaiian mantle plume.

In this paper we present new data on melt inclusions in olivine phenocrysts from picritic MORB from the Siqueiros Transform Fault on the northern EPR (Perfit et al. 1996). We suggest that coupled UDM and 'ghost plagioclase' signatures in MORB melt inclusions reflect localised processes of assimilation by primitive mantle-derived magmas of plagioclase-rich assemblages at crustal levels. The effects of crustal assimilation on compositions of oceanic lavas, resulting in unusually low contents of incompatible elements and positive Sr anomalies in some MORB and ophiolites, have been discussed previously (e.g. Elthon et al. 1986; Bedard 1993; Hemond et al. 1993; Bedard et al. 2000).

Analytical and modelling techniques

Major and minor elements in glasses and minerals were analysed on a Cameca SX50 electron microprobe at the University of Tasmania.

Glass and plagioclase were analysed at 15 kV, 20 nA, and a beam size of ~5 μm. International standards USNM 111240/2 (basaltic glass VG2) and USNM 119500 (plagioclase) from Jarosewich et al. (1980) were used as primary and secondary standards analysed throughout analytical sessions. Counting times for Na, Mg, Al, Si, Ca and Mn were 10 s for the peaks and 5 s for the backgrounds (10/5) on both sides. For Ti and Fe, counting times were 20/10, and for K, P and Cr they were 60/30. Olivine and spinel were analysed at 15 kV, 30 nA, and a beam size of 1–2 μm. International standards USNM 111312/444 (San Carlos olivine) and USNM 117075 (New Caledonia chromite) from Jarosewich et al. (1980) were used as primary and secondary standards analysed throughout analytical sessions. Counting times for Mg, Si, Fe and Al were 20/10; for Ca, Cr, Ni, Mn, V and Zn 30/15 for individual analyses and 60/30 for profiles through olivine. Detection limits for profiles are 0.010, 0.015 and 0.03 wt% for Ca, Cr and Ni, respectively. Each EMP analysis presented in this paper (except for profiles) is an average of two or three individual spots. Accuracy of the electron microprobe analysis at the above conditions varies from 2% for major elements to as much as 100% for absolute contents of 0.01 wt%. Chlorine and sulphur analyses were performed at 50 nA. Counting times for Cl were 180/180. Sulphur was analysed in the integrated mode using 19 steps of 25 s each between spectrometer position 61170 and 61710 on the PET crystal. At the above conditions detection limits for Cl and S are 40 and 150 ppm, respectively, and accuracy is better than 30 and 50%, respectively.

Trace element concentrations in melt inclusions and the matrix glass were analysed by laser ablation ICP-MS (inductively coupled plasma-mass spectrometry) at the Research School of Earth Sciences, ANU. This instrumentation comprises a Lambda Physik LPX120 ArF (193 nm) excimer laser coupled to an Agilent 7500S quadrupole ICPMS via an in-house designed laser ablation cell and transfer system. The analytical capabilities of this apparatus have been described elsewhere (Eggins et al. 1998a, 1998b), but have been modified and improved prior to this study particularly through deployment of the more sensitive Agilent 7500S quadrupole ICPMS. The melt inclusion analyses reported in this study were analysed by ablating 40-μm-diameter circular spots at a rate of ~0.5 μm/s (i.e. ~0.1-μm/laser pulse), except two larger inclusions and the matrix glass for which an 80-μm diameter spots were ablated. No variations exceeding the analytical uncertainty are observed between analyses with different beam sizes (Table 1). Data reduction was undertaken according to standard methods (Longerich et al. 1996) using the NIST612 glass as a primary reference material and the USGS BCR2g glass as a secondary reference material. The NIST 612 calibration values are reported in Table 1 along with concentration values obtained for BCR2 g. No corrections for interfering molecular or isobaric species were required due to the selection of appropriate analytical isotopes (see Table 1) and minimised molecular species formation (i.e. $^{+}ThO/^{+}Th < 0.5\%$).

Olivine fractional crystallisation on the walls of melt inclusions and its reverse, olivine addition to the melt from the walls, were simulated using the olivine–melt equilibrium model of Ford et al. (1983) following the algorithm of Danyushevsky et al. (2000). Fractionation of basaltic magma was simulated using the model of Danyushevsky (2001) at 0.1 GPa. All calculations, except for inclusion S2-OL54-GL, were performed using a Fe^{2+}/Fe^{3+} value of 9.52. This value was estimated based on the compositions of spinel from this sample (Table 2) after Maurel and Maurel (1982) using the technique of Danyushevsky and Sobolev (1996). The composition S2-OL54-GL was recalculated using Fe^{2+}/Fe^{3+} value of 6.99 because spinel included in this inclusion is more oxidised (Table 2). PC software PETROLOG used to perform the calculations is available from the first author on request.

Sample location and description

Fresh, unusually primitive, olivine-phyric basalts were collected in 1991 from the Siqueiros Transform Fault between intra-transform spreading centres with the submersible Alvin and by dredging (Perfit et al. 1996). The Siqueiros Transform Fault is located on the northern East Pacific Rise (EPR) between 8°20′N and 8°30′N along the Pacific and Cocos Plate boundary. The Siqueiros transform domain consists of three intra-transform spreading centres, A, B and C, which are connected by four left lateral strike slip faults striking approximately parallel to the transform boundary (Pockalny et al. 1997). Sample ALV-2384-3 was one of a

Table 1 Trace element contents in melt inclusion glasses (ppm). *1* Pillow rim glass of sample ALV-2384; *2–13* 'normal' melt inclusions; *11, 12* repeat analyses of inclusions 8 and 9 with 80 μm beam; *14, 15* intermediately depleted melt inclusions; *16* the most depleted melt inclusion; *17, 18* 'normal' melt inclusions with high Sr anomalies; *19* calibration values; *20* average of six analyses

No.	1	2	3	4	5	6	7	8	9	10	11	12	13	14	15	16	17	18	19	20
Sample	ALV-2384-3	S1-OL14-GL2	S1-OL20-GL	S1-OL48-GL2	S1-OL63-GL	S2-OL4-GL	S2-OL58-GL	S2-OL104-GL	S2-OL141-GL1	S2-OL141-GL2	S2-OL141-GL1-l.s.	S2-OL104-GL-l.s.	S1-OL24-GL1	S1-OL24-GL2-SP	S1-OL24-GL3-SP	S2-OL54-GL-SP	S1-OL59-GL1	S2-OL13-GL	NIST 612	BCR2g
Rb	0.126	0.049	0.228	0.081	0.138	0.055	0.146	0.138	0.156	0.084	0.135	0.137	0.334	0.025	0.037	< 0.055	0.492	0.059	32	56.2
Ba	1.30	0.872	2.03	0.846	1.12	0.804	1.51	1.47	1.45	1.19	1.44	1.51	2.77	0.417	0.392	0.164	4.69	1.15	38.5	675
Th	0.030	0.031	0.051	0.015	0.029	0.020	0.031	0.031	0.023	0.018	0.032	0.040	0.056	< 0.009	< 0.012	< 0.015	0.114	0.011	37.8	5.77
U	0.016	0.013	< 0.015	< 0.021	0.021	0.012	0.011	0.027	0.019	0.023	0.018	0.017	0.041	< 0.012	< 0.009	< 0.015	0.034	< 0.009	37.4	1.76
Nb	0.523	0.435	0.707	0.408	0.502	0.384	0.544	0.654	0.579	0.512	0.547	0.630	0.820	0.084	0.083	< 0.014	1.46	0.120	42	13.1
Ta	0.041	0.032	0.070	0.035	0.043	0.024	0.042	0.034	0.045	0.034	0.040	0.050	0.065	0.011	0.016	< 0.015	0.110	< 0.009	41	0.780
La	1.16	1.06	1.40	1.29	1.10	0.912	1.23	1.52	1.23	1.20	1.21	1.45	1.41	0.258	0.199	0.052	2.60	1.00	36	25.0
Ce	4.40	3.77	4.73	4.92	4.12	3.70	4.34	5.08	4.57	4.40	4.41	5.15	3.88	0.979	0.815	0.169	6.49	4.97	38	53.0
Sr	81.8	68.0	102	110	80.3	75.1	76.8	84.4	77.4	85.3	78.1	84.7	95.5	149	146	101	166	173	78	340
Nd	5.23	4.46	5.11	5.56	4.74	5.40	5.23	4.98	4.97	5.80	5.02	5.08	4.41	1.24	1.03	0.269	5.10	5.95	35	28.0
Zr	47.7	35.4	47.5	50.8	39.4	40.2	40.6	44.3	41.9	45.2	41.7	44.1	32.6	8.3	6.7	1.11	46.5	49.1	40	184
Hf	1.54	1.08	1.43	1.40	1.27	1.33	1.25	1.40	1.35	1.31	1.29	1.33	1.00	0.273	0.212	< 0.05	1.51	1.52	37	4.75
Sm	2.32	1.83	1.73	2.49	2.06	2.26	2.31	1.95	2.25	2.38	2.10	1.99	1.92	0.764	0.510	0.117	2.09	2.11	38	6.55
Ti	6,012	5,021	5,520	6,913	5,456	5,802	5,676	5,001	5,527	6,220	5,493	4,936	5,250	2,273	1,776	336	5,531	6,249	41	13,673
Eu	0.952	0.783	0.766	1.21	0.823	0.950	0.917	0.827	0.866	0.969	0.850	0.845	0.820	0.409	0.415	0.172	0.831	0.976	36	1.92
Gd	3.40	2.84	2.99	3.96	3.12	3.12	3.33	3.01	3.21	3.65	3.10	3.11	3.122	1.358	1.121	0.178	3.00	3.45	38	6.60
Dy	4.051	3.61	3.73	4.83	3.82	3.80	4.23	4.09	3.95	4.05	3.85	4.02	4.055	2.937	2.281	0.336	3.65	4.20	36	6.17
Er	2.49	2.15	2.68	2.48	2.47	2.38	2.47	2.60	2.49	2.46	2.45	2.51	2.600	2.422	2.130	0.240	2.57	2.52	38.5	3.53
Y	23.9	21.9	24.1	27.5	23.2	22.7	24.1	24.1	23.1	24.8	23.0	23.8	24.3	21.4	18.6	1.93	22.8	24.0	42	35.7
Yb	2.32	2.01	2.31	2.32	2.18	2.19	2.35	2.35	2.26	2.39	2.22	2.29	2.53	2.49	2.34	0.343	2.13	2.30	39	3.29

Table 2 Compositions of spinel inclusions in olivine phenocrysts from sample ALV-2384-3 (wt%). FeO* All iron as FeO; FeO and Fe_2O_3 contents are calculated according to stoichiometry; *MgN* 100*Mg/(Mg+Fe); *CrN* 100*Cr/(Cr+Al)

Sample	S2-OL54-GL-SP	S1-OL24-GL2-SP	S1-OL24-GL3-SP	S1-OL1-SP	S1-OL10-SP	S1-OL14-GL-SP1	S1-OL14-GL-SP2	S1-OL22-SP	S1-OL59-SP1	S2-OL158-SP	S2-OL1-SP	S2-OL5-SP	S2-OL11-SP	S2-OL58-SP	S2-OL155-SP1	S2-OL155-SP2
SiO_2	0.13	0.16	0.14	0.13	0.13	0.13	0.10	0.12	0.13	0.16	0.15	0.17	0.14	0.16	0.14	0.12
TiO_2	0.01	0.09	0.05	0.26	0.30	0.28	0.31	0.23	0.29	0.28	0.30	0.29	0.27	0.29	0.24	0.24
Al_2O_3	62.90	45.87	48.10	43.05	37.44	38.23	37.16	42.71	38.71	38.35	37.21	38.20	41.34	38.32	41.95	41.91
FeO*	9.18	11.88	11.32	12.25	12.65	12.92	13.04	12.15	12.65	12.06	12.49	12.69	12.19	12.58	12.22	12.21
MnO	0.07	0.08	0.07	0.09	0.07	0.07	0.09	0.08	0.09	0.07	0.07	0.07	0.08	0.06	0.06	0.07
MgO	22.23	19.89	20.22	19.38	18.72	18.49	18.39	19.46	18.88	19.05	18.73	18.68	18.87	18.83	19.36	19.41
CaO	0.06	0.12	0.04	0.01	0.00	0.03	0.05	0.01	0.03	0.00	0.01	0.02	0.02	0.00	0.00	0.01
Cr_2O_3	2.80	20.35	18.15	23.06	28.86	27.75	29.23	23.57	27.23	28.38	29.34	27.43	24.41	28.35	24.80	24.50
NiO	0.35	0.29	0.30	0.27	0.27	0.29	0.26	0.27	0.26	0.31	0.27	0.29	0.26	0.30	0.29	0.28
V_2O_3	0.01	0.09	0.11	0.14	0.15	0.12	0.13	0.09	0.10	0.11	0.14	0.08	0.12	0.12	0.12	0.04
ZnO	1.43	0.03	0.07	0.08	0.08	0.05	0.05	0.04	0.07	0.05	0.14	0.04	0.02	0.13	0.00	0.08
Fe_2O_3	3.39	3.97	3.63	3.81	4.07	3.99	4.02	3.89	4.24	3.75	3.93	4.12	3.46	3.89	3.68	3.98
FeO	6.12	8.31	8.05	8.82	8.99	9.33	9.43	8.65	8.84	8.69	8.96	8.98	9.07	9.08	8.91	8.62
Fe^{2+}/Fe^{3+}	2.00	2.33	2.46	2.57	2.45	2.59	2.61	2.47	2.32	2.58	2.54	2.42	2.91	2.59	2.69	2.41
MgN	86.62	81.01	81.74	79.67	78.78	77.95	77.66	80.05	79.21	79.63	78.84	78.75	78.76	78.72	79.48	80.05
CrN	2.90	22.94	20.20	26.43	34.08	32.75	34.54	27.02	32.06	33.18	34.59	32.50	28.37	33.17	28.40	28.17
Host Fo	90.03	90.56	90.36	90.30	90.75	90.53	90.53	90.37	90.58	90.97	90.74	90.57	90.26	90.73	90.43	90.43

number of picritic basalts recovered during Alvin dive 2384 from a fresh lava flow present along the A–B strike-slip fault at a depth of 3,751 m. This sample (Table 3) contains ~10% of euhedral to subhedral olivine phenocrysts 1–3 mm in size, and rare, small (< 1 mm) plagioclase phenocrysts with subhedral to irregular shapes. Other picritic lavas from the same area also contain small plagioclase crystals which generally constitute ≪1 vol% of the samples. More evolved plagioclase + olivine phyric lavas recovered during dive 2384 contain small millimetre-sized gabbroic xenoliths that range in composition from troctolites to olivine gabbros.

Compositions of olivine phenocryst cores in sample ALV-2384-3 range from $Fo_{89.3}$ to $Fo_{91.2}$ (54 grains analysed). Phenocrysts are either unzoned or have weak (< 0.3 Fo) reverse and normal zoning. Thin (~40 μm), normally zoned rims of up to 0.4 Fo present on all phenocrysts. Olivines contain abundant primary melt and spinel inclusions (Fig. 1a). Spinel is present as separate solid inclusions and in composite melt–spinel inclusions. Rare primary CO_2-rich fluid and sulphide inclusions are also present, indicating fluid and sulphide melt saturation of the crystallising magma.

Compositions of plagioclase phenocryst cores display a bimodal distribution. Most compositions range from An_{80} to An_{90}, whereas ~25% of all grains analysed (34 in total) have compositions between $An_{57–63}$. All grains contain numerous variably shaped melt inclusions that range in size from a few to several hundred microns. The low-An grains also contain primary low-density fluid inclusions.

Olivine and spinel are the only phases on the liquidus of the high-Mg pillow-rim glasses from the Siqueiros Transform, including glass of sample ALV-2384-3 (Perfit et al. 1996). This is demonstrated on Fig. 2a, where Al_2O_3 contents of glasses with MgO > 9 wt% increase with decreasing MgO. Modelling of low-pressure crystallisation of glass composition ALV-2384-3 (MgO = 9.6 wt%) indicates that plagioclase appears on the liquidus at ~9.2 wt% MgO (Fig. 2a). The estimated composition of plagioclase at the onset of its crystallisation (~An_{83}, Fig. 2a) is within the high-An compositional group of phenocrysts in sample ALV-2384-3. The calculated composition of olivine on the liquidus of glass ALV-2384-3 is $Fo_{88.6}$ (Table 3), indicating that most olivine phenocrysts in this sample crystallised from more primitive melts.

Melt inclusions in olivine phenocrysts

Melt inclusions in olivine phenocrysts are glassy, generally rounded in shape and vary in size from a few to ~200 μm (Fig. 1a). Shrinkage bubbles were only observed in a few large inclusions. The MgO content of the inclusion glasses ranges from that of the pillow-rim glass of sample ALV-2384-3 in larger inclusions, to significantly lower values (< 6 wt%) in smaller inclusions

Table 3 Major element compositions of melt inclusions in olivine phenocrysts from sample ALV-2384-3 (wt%). *FeO** All iron as FeO; *WR* whole rock composition from Perfit et al. (1996); GL – pillow-rim glass; I – melt inclusions

Sample	ALV-2384-3	ALV-2384-3	S1-OL14-GL2	S1-OL20-GL	S1-OL48-GL2	S1-OL59-GL1	S1-OL63-GL	S2-OL4-GL	S2-OL13-GL	S2-OL58-GL	S2-OL104-GL	S2-OL141-GL1	S2-OL141-GL2	S2-OL54-GL-SP	S1-OL24-GL1	S1-OL24-GL2-SP	S1-OL24-GL3-SP
	WR	GL	I	I	I	I	I	I	I	I	I	I	I	I	I	I	I
SiO_2	47.9	49.08	49.59	49.95	49.32	49.66	49.66	49.32	49.77	49.18	49.50	49.62	49.53	48.20	50.77	49.67	49.41
TiO_2	0.85	0.99	0.85	0.90	1.12	0.92	0.89	0.96	1.05	0.95	0.82	0.96	1.03	0.04	0.86	0.35	0.29
Al_2O_3	16.18	17.12	17.49	19.25	19.29	17.53	17.87	18.20	18.31	17.88	17.40	17.75	18.23	20.20	19.84	20.68	19.93
FeO*	7.92	8.04	8.23	7.62	7.59	7.79	7.61	7.88	7.33	8.01	7.90	7.76	8.20	7.77	7.31	7.20	7.74
MnO	0.1	0.17	0.17	0.16	0.14	0.15	0.15	0.15	0.15	0.14	0.13	0.17	0.13	0.10	0.16	0.15	0.15
MgO	14.24	9.58	7.48	5.61	5.54	9.57	9.21	8.71	8.33	8.30	8.56	9.17	7.38	7.47	4.80	4.94	5.68
CaO	10.64	12.36	13.24	14.18	14.40	12.64	12.88	13.15	13.37	13.48	13.80	12.95	13.38	14.61	15.27	16.05	16.05
Na_2O	2.16	2.33	2.06	2.24	2.42	2.18	2.24	2.26	2.34	2.18	1.92	2.18	2.35	1.06	2.27	1.73	1.48
K_2O	0.03	0.026	0.026	0.021	0.022	0.079	0.030	0.017	0.013	0.022	0.037	0.032	0.021	0.003	0.041	0.017	0.013
P_2O_5	0.07	0.029	0.062	0.038	0.063	0.131	0.038	0.022	0.005	0.027	0.050	0.047	0.048	0.022	0.036	0.002	0.000
Cr_2O_3		0.056	0.066	0.053	0.080	0.065	0.079	0.059	0.047	0.083	0.080	0.076	0.039	0.019	0.056	0.052	0.034
S		0.107	0.097	0.113	0.113	0.105	0.105	0.113	0.017	0.092	0.101	0.098	0.112	0.015	0.098	0.039	0.019
Cl ppm		< 40	< 40	< 40	< 40	< 40	< 40	< 40	< 40	< 40	< 40	43(8)	< 40	181(4)	52(39)	< 40	< 40
Total	100.09	99.88	99.35	100.13	100.10	100.82	100.77	100.85	100.74	100.36	100.30	100.81	100.45	99.52	101.50	100.87	100.79
Recalculated inclusion compositions																	
SiO_2			48.89	48.50	47.95	48.91	48.86	48.41	48.71	48.26	48.77	48.78	48.28	47.73	48.42	47.79	47.67
TiO_2			0.76	0.76	0.95	0.87	0.84	0.89	0.96	0.86	0.76	0.90	0.90	0.04	0.71	0.29	0.24
Al_2O_3			15.64	16.38	16.33	16.60	16.79	16.86	16.70	16.16	16.14	16.61	15.94	18.47	16.28	17.17	16.70
FeO*			8.67	8.34	8.29	7.84	7.69	8.00	7.50	8.23	8.08	7.84	8.56	8.13	8.15	8.03	8.42
MnO			0.17	0.16	0.15	0.15	0.15	0.15	0.15	0.14	0.13	0.17	0.14	0.11	0.16	0.15	0.15
MgO			11.99	11.74	11.89	11.32	11.32	11.31	11.56	12.02	11.36	11.37	12.31	11.11	11.71	11.68	12.01
CaO			11.88	12.11	12.24	11.98	12.11	12.20	12.22	12.22	12.81	12.14	11.73	13.39	12.59	13.38	13.51
Na_2O			1.84	1.90	2.05	2.07	2.11	2.09	2.14	1.97	1.78	2.04	2.05	0.97	1.86	1.43	1.24
K_2O			0.023	0.018	0.019	0.074	0.028	0.016	0.012	0.020	0.034	0.030	0.018	0.003	0.033	0.014	0.011
P_2O_5			0.055	0.032	0.053	0.124	0.036	0.021	0.005	0.024	0.046	0.044	0.042	0.020	0.029	0.001	0.000
Cr_2O_3			0.067	0.055	0.077	0.065	0.078	0.060	0.049	0.082	0.079	0.075	0.042	0.023	0.056	0.053	0.038
Ol wt%[a]			11.44	14.97	15.37	4.64	5.46	6.84	8.33	9.59	7.25	5.80	12.49	9.22	16.63	16.20	15.52
Host olivine																	
SiO_2			40.22	40.79	40.57	40.86	40.87	40.71	40.85	40.53	40.53	41.00	40.73	40.89	40.67	41.02	40.53
FeO*			9.58	9.54	9.14	9.31	9.12	9.38	8.67	9.06	9.54	9.25	9.25	9.60	9.25	9.19	9.30
MnO			0.18	0.15	0.16	0.16	0.15	0.16	0.15	0.15	0.16	0.16	0.15	0.15	0.15	0.17	0.16
MgO			48.26	49.42	49.11	49.54	49.65	49.32	49.94	49.31	49.22	49.54	49.40	48.61	49.26	49.44	48.94
CaO			0.28	0.30	0.30	0.30	0.29	0.29	0.30	0.29	0.29	0.29	0.29	0.29	0.31	0.34	0.33
Cr_2O_3			0.05	0.07	0.07	0.07	0.07	0.04	0.09	0.07	0.05	0.07	0.06	0.05	0.06	0.05	0.06
NiO			0.31	0.33	0.34	0.34	0.36	0.34	0.40	0.35	0.34	0.36	0.36	0.32	0.31	0.33	0.32
Fo		88.6[b]	89.98	90.23	90.55	90.46	90.66	90.36	91.13	90.65	90.20	90.52	90.50	90.03	90.47	90.56	90.36

[a]Amount of olivine added during calculations
[b]Calculated olivine composition in equilibrium with the glass

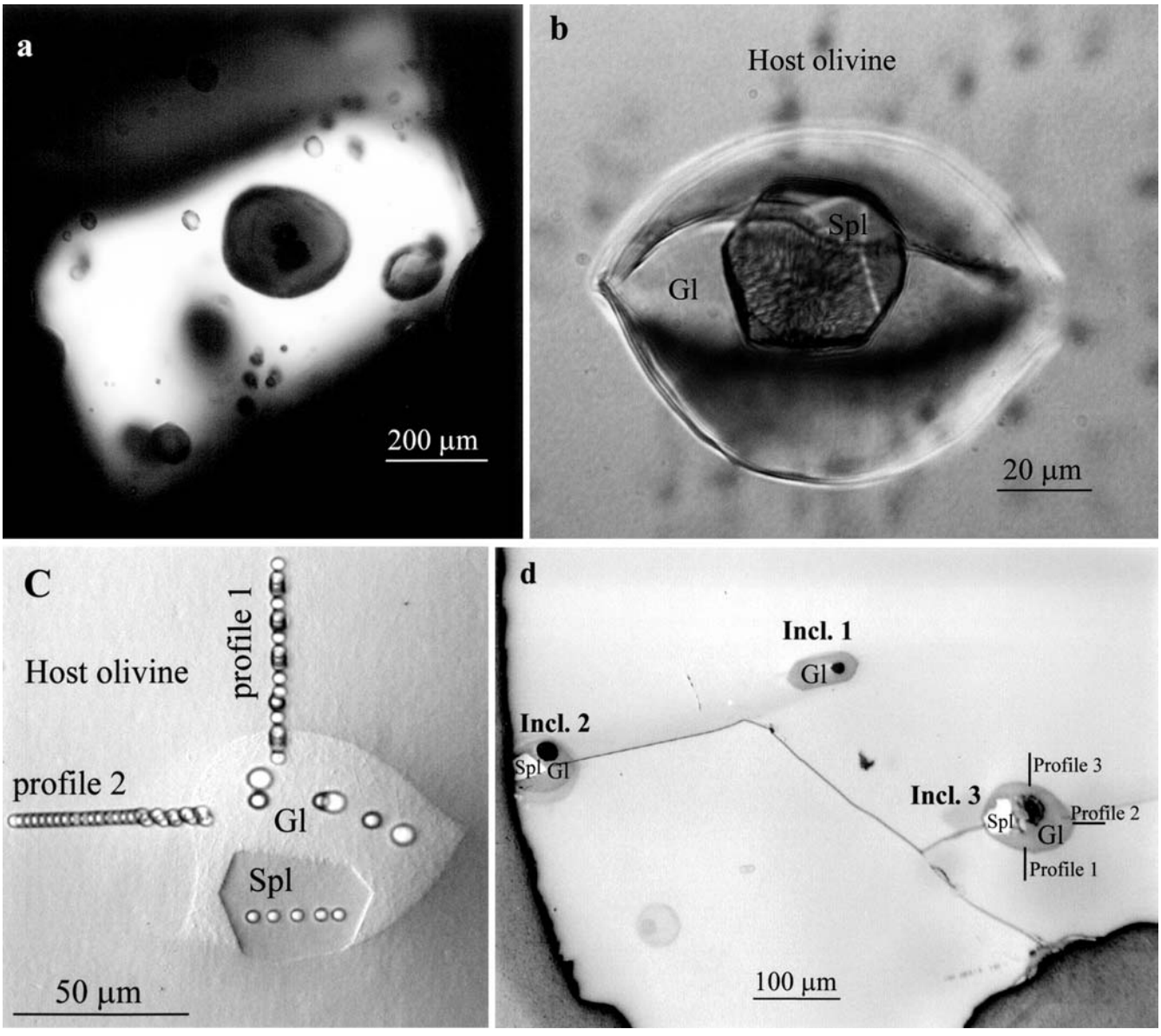

Fig. 1 **a** Olivine phenocryst S1-OL1 from sample ALV-2384-3 ($Fo_{90.3}$) with glassy melt inclusions. Note a shrinkage bubble and a spinel crystal inside the largest inclusion; **b** melt inclusion in olivine phenocryst S2-OL54 from sample ALV-2384-3 containing a large euhedral crystal of high-Al spinel. *Gl* Glass; *Spl* spinel. **c** The same inclusion as on **b**, exposed to the surface and carbon coated; *rounded spots* mark the placing of the electron microprobe analyses. **d** Melt inclusions in olivine phenocryst S1-OL24 from sample ALV-2384-3. *Gl* Glass; *Spl* spinel. Compositions of olivine along profiles on **c**, **d** are shown on Fig. 4c, d

(Table 3, Fig. 2). The observed range of MgO contents does not represent variations of the trapped melt compositions, but reflects variable extent of quench modification of inclusions (crystallisation of olivine on the walls of the inclusions) upon eruption. This is best demonstrated by the correlation between MgO and $Kd_{(Fe–Mg)}$ calculated for the host olivine and the residual melt (glass) inside the inclusions (Fig. 2c). Olivine crystallisation on the walls of the inclusions also explains large compositional differences between inclusion glasses and pillow-rim glasses from the Siqueiros Transform at MgO <9 wt% (Fig. 2a, b). Along the fractionation trend recorded by pillow-rim glasses, first olivine, then plagioclase and later clinopyroxene were the liquidus phases, whereas inside melt inclusions only olivine crystallised on their walls. Crystallisation along an olivine–plagioclase cotectic decreases Al_2O_3 and ncreases FeO* contents of the melt, whereas olivine-only crystallisation increases melt Al_2O_3 contents, and has little effect on melt FeO* contents (Fig. 2a, b).

Low Kd values for the most magnesian inclusions ($\sim$0.26), which have MgO contents similar to that of the pillow-rim glass of the sample, indicate that such inclusions also experienced some crystallisation of olivine on their walls, and that the trapped melt composition was more magnesian than the pillow-rim glass of the sample.

The trapped compositions of melt inclusions were estimated from the compositions of the residual glasses

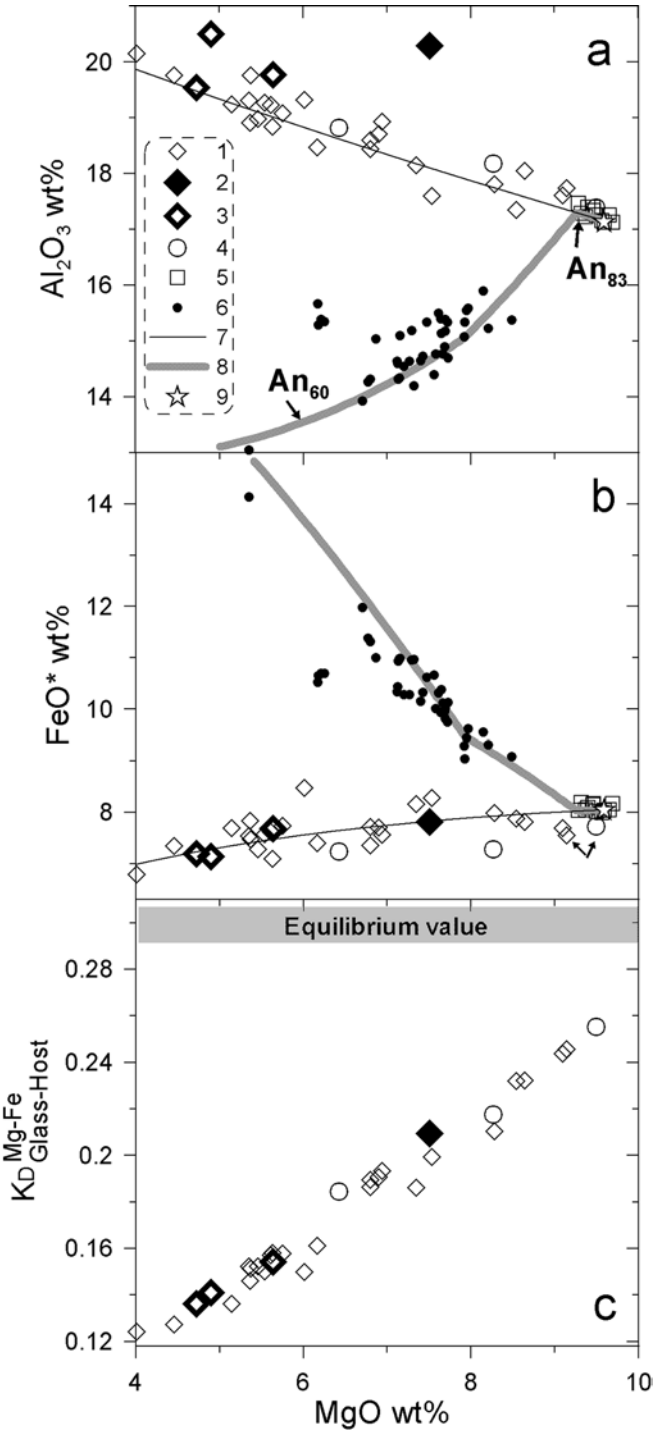

Fig. 2 **a** Al_2O_3 contents of naturally quenched glassy melt inclusions in olivine phenocrysts from sample ALV-2384-3. 1 'Normal' melt inclusions. 2 Inclusion in olivine S2-OL54. 3 Inclusions in olivine S1-OL24. 4 Inclusions with 'normal' concentrations of middle and heavy REE, relatively depleted or enriched highly incompatible elements, and substantial positive Sr anomalies (Fig. 5b). 5 Pillow-rim glasses recovered during dive ALV-2384 and dredge A2-D20. 6 Other pillow-rim glasses from within the Siqueiros transform. 7 Olivine fractionation trend calculated from the composition of the pillow-rim glass of sample ALV-2384-3 (Table 3). 8 Fractionation trend of the pillow-rim glass of sample ALV-2384-3; onset of plagioclase crystallisation corresponds to the decrease of Al_2O_3 content along the trend at ~9.2 wt% MgO; the calculated composition of plagioclase along the fractionation trend is indicated for the onset of plagioclase crystallisation (An_{83}) and for a more evolved composition (An_{60}). 9 The pillow-rim glass of sample ALV-2384-3. **b** FeO* contents of naturally quenched glassy melt inclusions in olivine phenocrysts from sample ALV-2384-3; *symbols* as on Fig. 2a; *arrows* indicate inclusions for which compositional profiles were analysed through the surrounding olivine. **c** Correlation between MgO and $Kd_{(Fe-Mg)}$ calculated for the host olivine and the residual melt (glass) inside the inclusions; symbols as on Fig. 2a. See text for discussion

by modelling the reverse of olivine crystallisation on the walls of the inclusions. The calculated trapped compositions are shown in Table 3 and Fig. 3. Modelling of the reverse of olivine crystallisation for each inclusion continued until the melt composition reached equilibrium with the host olivine, according to the model of Ford et al. (1983).

When applying this technique, it is important to assess the extent of post-entrapment re-equilibration between melt inclusions and their hosts. Such re-equilibration, called 'Fe-loss', results in lower FeO* contents and artificially high Mg# of the residual melt inside inclusions and, if not accounted for, causes underestimation of the amount of olivine crystallised on the inclusion walls (see Danyushevsky et al. 2000 for more details). The Al_2O_3 and FeO* contents of the residual melt inside inclusions (glass) generally follow the olivine fractionation trend calculated from the composition of the host glass (Fig. 2a, b), indicating that no significant 'Fe-loss' occurred. The lack of significant re-equilibration is also demonstrated by the compositional profiles in olivine adjacent to melt inclusions, measured for inclusions with relatively low glass FeO* contents (Figs. 2b, 4a, b). The width of the diffusion profiles is 10–14 μm, corresponding to a decrease in the FeO* content of the residual melt inside these inclusions of <0.4 wt% FeO. This value is close to the analytical uncertainty, and is within the scatter of FeO* contents in melt inclusion glasses at a given MgO (Fig. 2b). Thus no correction for Fe-loss have been introduced.

Estimated trapped melt compositions have 11–12.5 wt% MgO (Fig. 3), and calculated crystallisation temperatures of olivine phenocrysts (i.e. olivine liquidus temperatures of the trapped inclusion compositions) are $1{,}275 \pm 11$ °C.

Compositions of parental melts for pillow-rim glass ALV-2384-3 can be estimated by modelling the reverse of olivine fractionation (bold solid line on Fig. 3). Despite some scatter, major element contents in most of the inclusions (called hereafter 'normal' inclusions) generally follow the calculated trend and, thus, are consistent with being representative of the parental melts. However, several inclusions are clearly different and have significantly lower TiO_2 and Na_2O, and higher CaO, Al_2O_3 or K_2O contents. Incompatible element contents of 'normal' melt inclusions (Table 1, Fig. 5) are similar to those of the pillow-rim glass, whereas melt inclusions with different major element chemistry also have

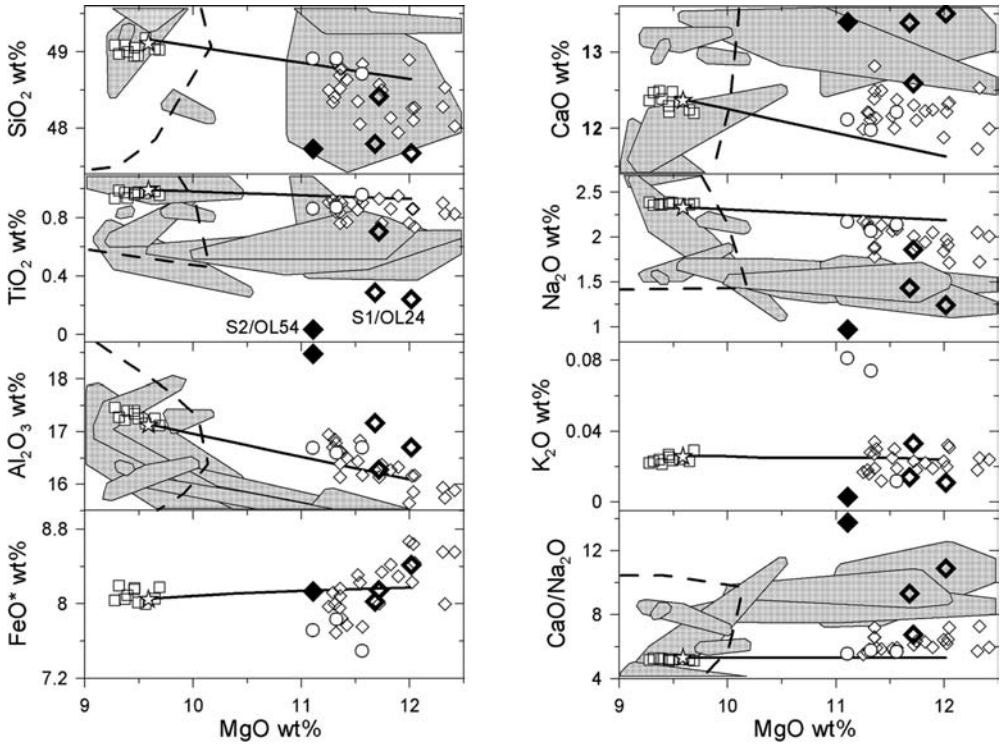

Fig. 3 Compositions of melt inclusions in olivine phenocrysts from sample ALV-2384-3, recalculated to be in equilibrium with the host olivine. *Symbols* as on Fig. 2. *Solid black line* represents the reverse olivine fractionation trend calculated from the composition of the pillow-rim glass of sample ALV-2384-3 (Table 3). The field outlined by a *thick dashed line* shows primitive MORB pillow-rim glasses from different localities from the Smithsonian Institution catalogue (http://www.nmnh.si.edu/minsci/research/glass/index.htm) and our data. *Grey fields* show compositions of melt inclusions in primitive MORB olivine, plagioclase and spinel phenocrysts from Danyushevsky et al. (1988); Sobolev et al. (1989); Gurenko and Chaussidon (1995); Kamenetsky (1996); McNeill (1997); Kamenetsky et al. (1998); and our unpublished data (each location is shown separately). See text for discussion

different incompatible element patterns. These unusual inclusions, which comprise less than a few percent of the inclusion population in sample ALV-2384-3, are described in detail below.

Olivine phenocryst S2-OL54

Phenocryst S2-OL54 has a large (~1 mm) unzoned core of $Fo_{90.0}$ surrounded by a reversely zoned ($Fo_{90.0–90.4}$) area 150–200 μm thick, and by a thin (~20 μm) normally zoned outer rim (down to $Fo_{\sim 90}$), which is similar to other olivine phenocrysts from this sample. Mn, Ca, Cr and Ni contents are also within the range of other olivines. This phenocryst contains a single glassy melt inclusion (~60 μm in diameter; Fig. 1b) situated in the unzoned core. The melt inclusion contains a large euhedral crystal of high-Al spinel (~25 μm; Fig. 1b). The major element compositions of the host olivine and glass are presented in Table 3, trace elements in the glass in Table 1, and spinel composition in Table 2.

The composition of the glass is very unusual. Compared with melt inclusions in primitive MORB phenocrysts reported to date (Fig. 3), it has a very high Al_2O_3 content, very low TiO_2 and Na_2O concentrations, and a very high CaO/Na_2O value. Compared with 'normal' inclusions from sample ALV-2384-3, it also has high CaO and Cl content and low SiO_2, K_2O, Cr_2O_3 and S. Contents of all incompatible elements, except for Sr, are extremely low. The primitive mantle-normalised trace element pattern of this inclusion (Fig. 5a) shows it to have a very large positive Sr anomaly and it is also characterised by a positive Eu anomaly and negative Zr and Hf anomalies.

The composition of spinel in this inclusion is also unusual. Compared with other spinels from this sample,

►

Fig. 4a–d Compositional profiles in olivine phenocrysts around melt inclusion from sample ALV-2384-3. Position of the glass/olivine boundary (*thick solid line*) is determined using stoichiometry (Danyushevsky et al. 2000). Analyses at the boundary are affected by the analytical overlap between glass and olivine. FeO* contents in olivine next to glass are higher than the analysed values (~11 wt% in **a**, **b**; ~13.5 wt% in **c**; ~17 wt% in **d**; all values are estimated from the olivine-melt equilibrium model of Ford et al. (1983) on the basis of the residual melt (i.e. glass) compositions). Width of the olivine rim on the walls of the inclusions (*dashed line*) is estimated from the calculated amount of olivine that crystallised on the walls after trapping (Table 3), assuming olivine density of 3.3 g/cm^3 and spherical shapes of the inclusions. Profiles were analysed on two or three sides of the inclusions and are symmetrical. **a** inclusion in olivine S1-OL59, radius 60 μm; **b** inclusion in olivine S1-OL63, radius 50 μm; **c** inclusion in olivine S2-OL54, radius 30 μm; position of profiles 1 and 2 relative to the inclusion is shown on Fig. 1c; **d** inclusion 3 in olivine S1-OL24, radius 60 μm; position of profiles 1, 2 and 3 relative to the inclusion is shown on Fig. 1d. See text for discussion

and spinels from other MORB (Fig. 6), it has very high Al_2O_3 and low TiO_2 contents. Inclusions of high-Al spinel in olivine phenocrysts have been described in subduction-related volcanics (Della-Pasqua et al. 1995) and ophiolites (Bedard and Hebert 1998), but to our knowledge they have not been reported in present day MORB. The above compositional features of this spinel are consistent with the high-Al_2O_3 and low-TiO_2 nature of the glass in the inclusion. This spinel has also a lower Fe^{2+}/Fe^{3+} value (estimated from stoichiometry) than other spinels from this sample (Table 2, Fig. 6) and has high ZnO content; an uncommon feature of MORB spinels.

Compositional profiles through olivine adjacent to the melt inclusion are shown in Fig. 4c and their position in Fig. 1c. Cr contents in olivine gradually increase

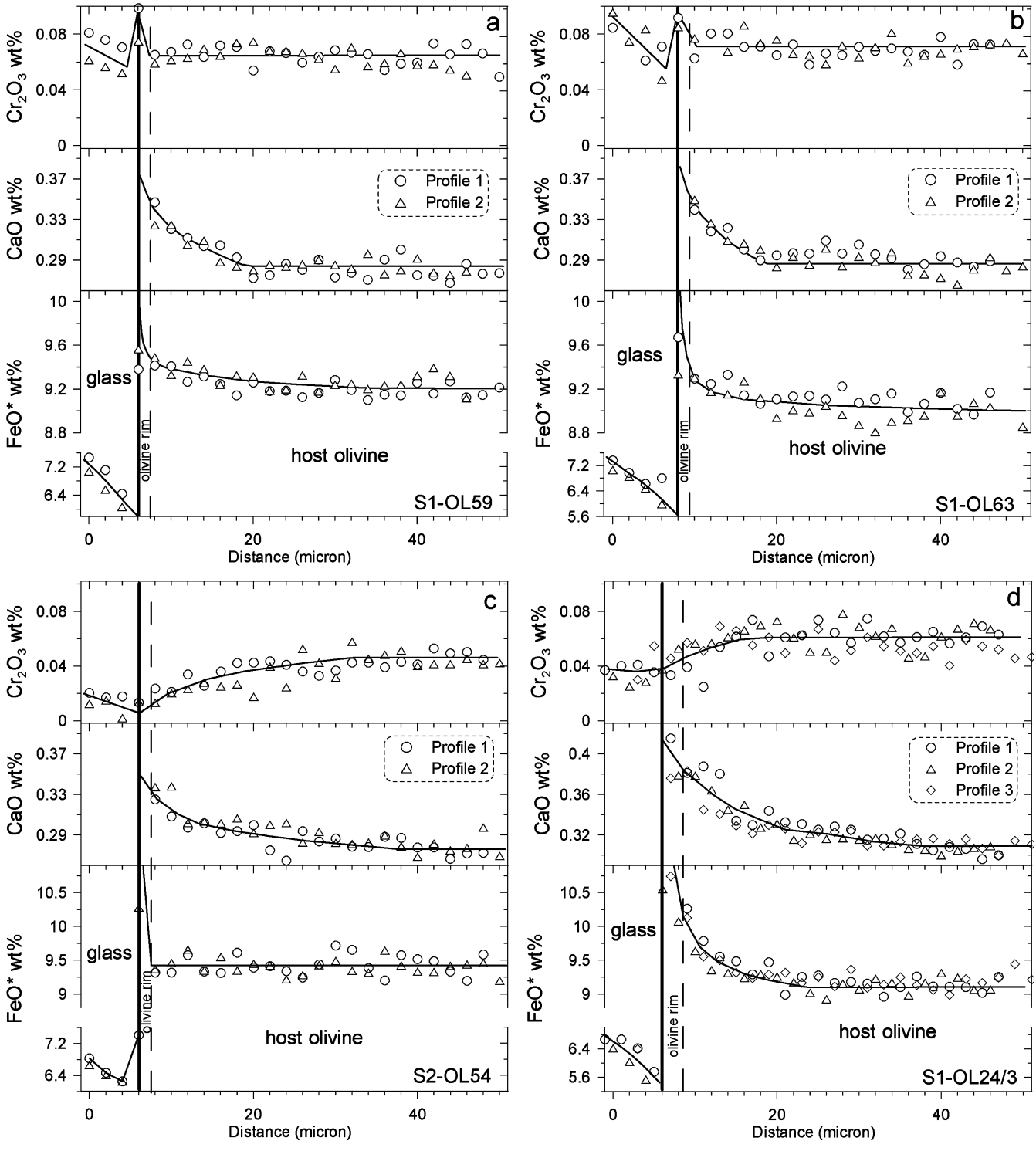

whereas Ca contents decrease away from the inclusion. Both reach background levels (the concentration of the phenocryst far away from the inclusion) at ~25–30 μm. This is quite different from what is observed around 'normal' inclusions (Fig. 4a, b), where diffusion profiles of Ca from inclusions are significantly shorter (< 10 μm), and Cr contents either increase slightly towards the inclusions or remain constant, and are significantly higher in the olivine rim. Also unlike 'normal' inclusions, Fe contents of olivine do not increase toward the inclusion.

Olivine phenocryst S1-OL24

Phenocryst S1-OL24 ($Fo_{\sim 90.5}$) contains several melt inclusions, three of which were analysed (Fig. 1d, Table 3). No compositional zoning was found in the host olivine between these inclusions. Inclusion 1 is a 'normal' inclusion (Figs. 3, 5; Tables 1, 3) whereas inclusions 2 and 3 have higher Al_2O_3 and Ca contents, and lower SiO_2, Na_2O, Cr_2O_3, S and incompatible element contents than normal inclusions. They also have large positive Sr anomalies, and small positive Eu and negative Zr and Hf anomalies. Many compositional features of these inclusions are intermediate between 'normal' inclusions and inclusion in phenocryst S2-OL54 described above.

Spinels inside inclusions 2 and 3 also have compositions intermediate between 'normal' spinels and the spinel inside melt inclusion in S2-OL54 (Fig. 6, Table 2). In particular, they have higher Al_2O_3 and lower TiO_2 contents than 'normal' spinels.

Compositional profiles through olivine around inclusions 2 and 3 also have 'intermediate' characteristics (Fig. 4d). Similar to olivine S2-OL54, there are well-defined diffusion profiles of Ca from the inclusions and Cr into the inclusions, although they are shorter (~15 μm) than those around the inclusion in S2-OL54. On the other hand, similar to the profiles around 'normal' inclusions, Fe contents in olivine clearly increase towards the inclusions. Compositional profiles around

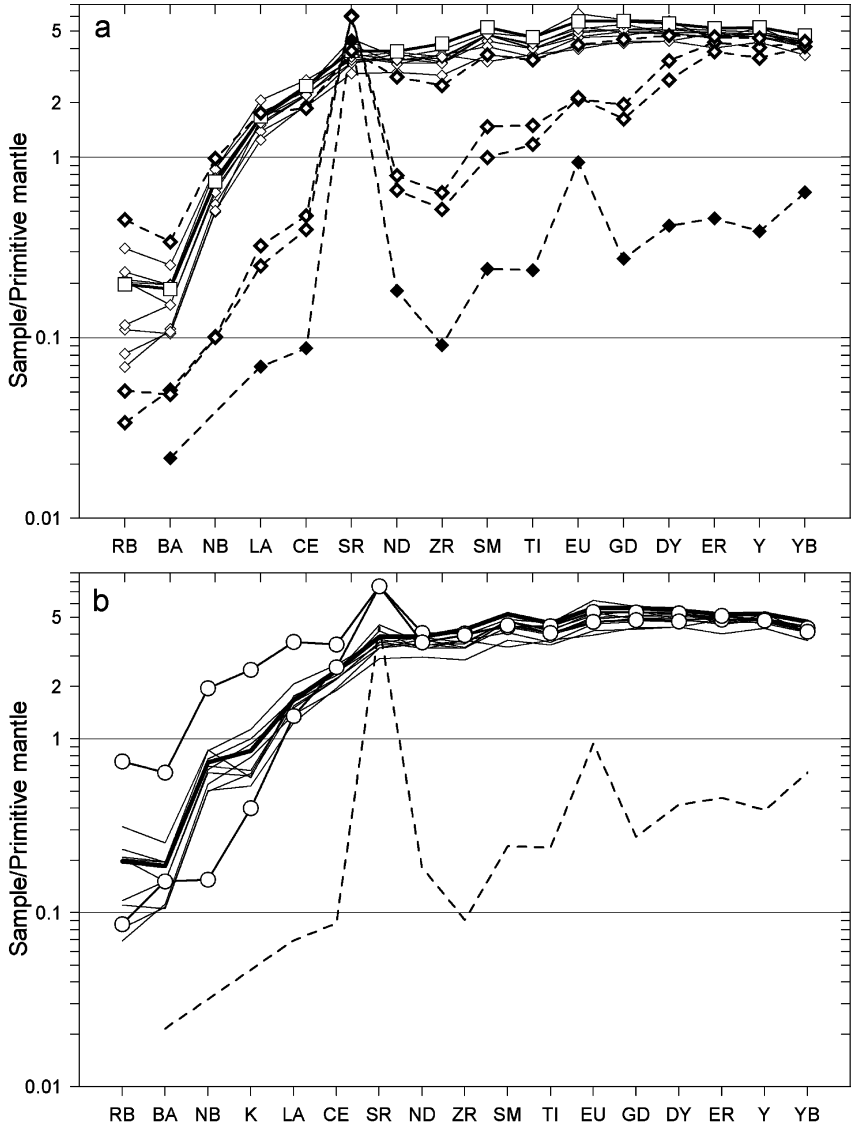

Fig. 5a, b Primitive mantle-normalised contents of trace elements in naturally quenched glassy melt inclusions from sample ALV-2384-3, corrected for crystallisation of olivine on the walls of the inclusions. The amount of olivine crystallised is shown in Table 3. Trace element concentrations in olivine are assumed to be 0. *Symbols* as on Fig. 2 *Dashed pattern* on **b** shows inclusion in olivine S2-OL54 from **a**; *bold solid pattern* shows pillow rim glass ALV-2384-3 from **a**; thin solid patterns without symbols show 'normal' inclusions from **a**. Normalisation values from Sun and McDonough (1989). See text for discussion

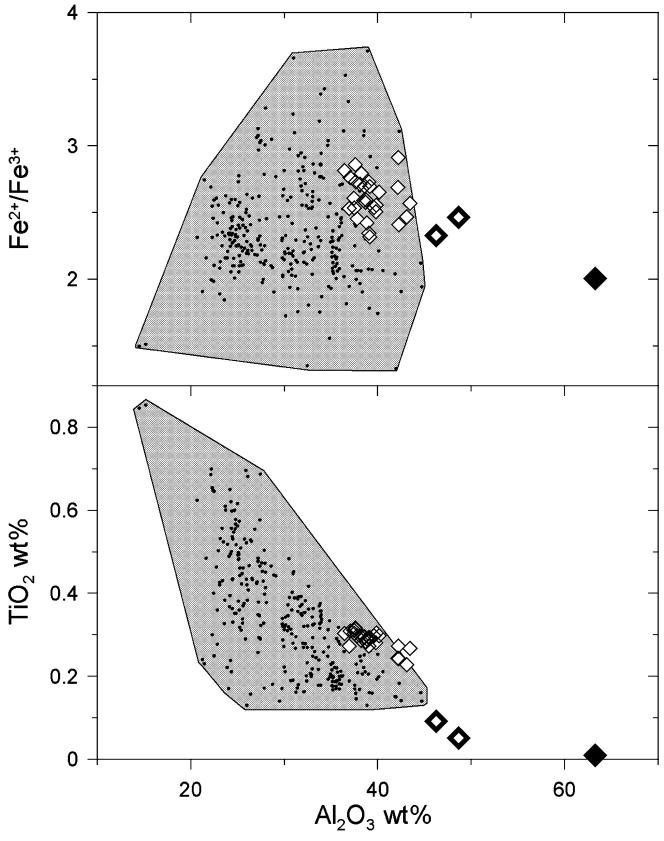

Fig. 6 Compositions of spinel phenocrysts and spinel inclusions in olivine phenocrysts from sample ALV-2384-3. *Filled diamond* Spinel inside melt inclusion in olivine S2-OL54; *large open diamonds* spinel inside melt inclusions 2 and 3 in olivine S1-OL24; *small open diamonds* other spinel from this sample; *grey field* compositions of spinel phenocrysts and inclusions in olivine and plagioclase phenocrysts in primitive MORB from different locations. with individual analyses shown as *small black* dots (Danyushevsky et al. 1988; Sobolev et al. 1989; Kamenetsky 1996; McNeill 1997; Kamenetsky et al. 1998; our unpublished data from Atlantic, Pacific and Indian ocean MORB). See text for discussion

inclusion 1 (not shown) are similar to those around other 'normal' melt inclusions (Fig. 4a, b).

Olivine phenocrysts S1-OL59 and S2-OL13

Major element contents of melt inclusions in these phenocrysts ($Fo_{90.5}$ and $Fo_{91.1}$, respectively) are similar to other 'normal' melt inclusions (Table 3, Fig. 3). Concentrations of trace elements more compatible than Sr are also similar to 'normal' inclusions (Fig. 5b, Table 1). However, unlike 'normal' inclusions, these two inclusions have substantial positive Sr anomalies. Sr contents of these melt inclusions are the highest among all melt inclusions analysed. Contents of highly incompatible elements in these inclusions also differ from 'normal' inclusions. The inclusion in olivine S2-OL13 is relatively depleted in highly incompatible elements, whereas the inclusion in S1-OL59 has higher contents of highly incompatible elements (a second inclusion in S1-OL59 also has high K_2O content (Fig. 3), but trace elements in this inclusion were not analysed due to its small size).

Discussion

Mineralogy of picritic basalt ALV-2384-3, which is fairly representative of others from the Siqueiros transform, suggests that it had a relatively complicated petrogenetic history. Both populations of plagioclase phenocrysts must have crystallised from more evolved melts than the erupted melt represented by the pillow-rim glass of the sample. As the glass composition is close to plagioclase saturation, and the estimated plagioclase composition at the onset of its crystallisation is within the high-An group (Fig. 2a), the high-An plagioclase phenocrysts may have crystallised in situ after the eruption. However, the low-An plagioclase crystallised from significantly more evolved melts (Fig. 2a) and, thus, these plagioclases are certainly xenocrystic. Olivine phenocrysts, on the other hand, crystallised from significantly more primitive melts, not represented among pillow-rim glasses recovered within the Siqueiros Transform.

In the discussion below we utilise the data obtained from melt inclusions in an attempt to unravel the magmatic events and to characterise different components that were involved in petrogenesis of these rocks.

Origin of the melt inclusion in olivine phenocryst S2-OL54

The combination of extremely low TiO_2 and Na_2O, and high Al_2O_3 contents of the melt in this inclusion, precludes its origin during melting of peridotite, wherlite or eclogite mantle assemblages. Moreover, the combination of the high Al_2O_3 content with strong positive Sr and Eu anomalies and a negative Zr anomaly suggests that plagioclase was a major component in the source of the melt, as plagioclase–melt distribution coefficients (Kd) for Sr and Eu are high, and for Zr and Hf are low compared with REE of similar incompatibility (e.g. Bindeman and Davis 2000). Similar compositional features of the melt and spinel in this inclusion (i.e. unusually high Al_2O_3 and low TiO_2 and Cr_2O_3 contents; Tables 2, 3, Figs. 3, 6) also suggest that they are likely to be cogenetic. Despite the unusual chemistry of the melt and spinel in this inclusion, major and minor element contents in the host olivine are within the tight range of other olivines from this sample (Table 3).

Understanding the origin of this inclusion relies on an understanding of the following: (1) if the melt and spinel were trapped together, or if the observed phases (spinel and melt) in the inclusion were formed after trapping; (2) if they were trapped together, are the observed proportions between melt and spinel, a random result of the trapping process, or the bulk composition of the

inclusion (residual melt + olivine rim on the walls + spinel) is representative of the source of the melt; (3) if the observed phases in the inclusion were formed after trapping, what was the original physical state of the inclusion (i.e. was it originally a single-phase melt inclusion, a single-phase or a multiple-phase crystalline inclusion, or a combination of melt and crystal(s) different to that observed in the inclusion now); and (4) was the host olivine phenocryst in equilibrium with the trapped material at the moment of trapping?

Compositional profiles through olivine adjacent to the inclusion (Fig. 4c) demonstrate that Cr diffuses from olivine into the inclusion. This is not observed around 'normal' melt inclusions (Fig. 4a, b), indicating that inclusion S2-OL54 did not have sufficient Cr_2O_3 content to be in equilibrium with the host. [Note that olivine and spinel on the liquidus of a high-Mg MORB melt with ~0.07 wt% Cr_2O_3 have ~0.06 wt% Cr_2O_3 and ~25 wt% Cr_2O_3, respectively (Table 3). In a composite melt + spinel inclusion with the above compositions, all phases are in equilibrium and no Cr diffusion will occur. In the case of inclusion S2-OL54, however, the normal Cr_2O_3 content of the host olivine is too high for the high-Al/low-Cr melt and spinel, and thus Cr diffused into the inclusion]. Thus, this is not a typical melt inclusion, in the sense that it does not represent the melt from which the host phenocryst grew. Similar to inclusions of spinel, fluid or sulphide globules, which are common in olivine phenocrysts in MORB, this inclusion represents a separate phase in the magma, but dissimilar to such inclusions, this phase was also foreign, i.e. it was not in equilibrium with the host olivine.

The bulk composition of the inclusion (glass, corrected for olivine fractionation on the walls, plus spinel) is presented in Table 4, no. 1. It was estimated assuming spherical shapes of the inclusion and spinel ($r = 30$ μm and 12.5 μm, respectively), and their densities of 2.65 and 4 g/cm^3, respectively. Resulting mass proportions of glass to spinel are 0.895/0.105. The normative components of the bulk inclusion composition are essentially plagioclase and olivine. As shown by experimental studies (e.g. Presnall et al. 1978; Onuma and Tohara 1983), such compositions melt incongruently at low pressure, producing high-Al spinel as the liquidus phase, and thus we suggest that an olivine–plagioclase assemblage was the precursor to this inclusion.

The trace element content of the bulk composition was calculated assuming spinel has negligible concentrations of the elements in question (note that $Kd^{Spl/Melt}$ values for the elements presented in Table 4 are very low (Green 1994; Horn et al. 1994; Garrido et al. 2000) and any resulting uncertainties in the bulk composition are well within the analytical and calculation errors). The trace element concentrations are very similar to some plagioclase-rich troctolites collected from the Garrett transform fault and Hess Deep, EPR and Oman ophiolite (Table 4; Benoit et al. 1996; Dick and Natland 1996; Constantin 1999), further supporting an olivine-plagioclase source for this inclusion.

Table 4 Calculated bulk compositions of inclusions in olivines S2-OL54 and S1-OL24, sample ALV-2384-3, and plagioclase-rich troctolites from lower oceanic crust. *1* Bulk composition of inclusion in olivine S2-OL54 (see text for calculation details); *2* sample 03-10 from Garrett Transform Fault (Constantin 1999); *3* sample 93-OG-67B from Oman ophiolite (Benoit et al. 1996); *4* sample 895E-1R-1, 70–75, 7B from Hess Deep (Falloon, unpublished data); *5* bulk composition of inclusion no. 3 in olivine S1-OL24 (see text for calculation details); *6* bulk composition of inclusion no. 2 in olivine S1-OL24 (see text for calculation details); *7* bulk composition of 'normal' inclusion no. 1 in olivine S1-OL24; all compositions are recalculated to 100 wt% anhydrous. *FeO** Total Fe as FeO; *MgN* 100*Mg/(Mg + Fe); *CaN* 100*Ca/(Ca + Na); *norms* CIPW norms in mol%; *Cor* Al_2O_3; *Per* (Mg,Fe)O

No.	1	2	3	4	5	6	7
wt%							
SiO_2	42.73	45.03	43.94	45.38	45.77	46.13	48.42
TiO_2	0.03	0.04	0.04	0.07	0.24	0.28	0.71
Al_2O_3	23.22	22.50	24.81	23.29	18.00	18.20	16.28
FeO*	8.25	4.30	3.03	4.23	8.54	8.17	8.15
MnO	0.10	0.05	0.04	0.05	0.15	0.15	0.16
MgO	12.30	15.45	15.14	13.79	12.36	11.98	11.71
CaO	11.99	11.14	12.09	12.10	12.97	12.92	12.59
Na_2O	0.87	1.03	0.88	0.91	1.19	1.38	1.86
K_2O	0.00	0.36	0.00	0.00	0.01	0.01	0.03
P_2O_5	0.02	0.06	0.00	0.01	0.00	0.00	0.03
Cr_2O_3	0.32	0.02	0.02	0.17	0.78	0.77	0.06
MgN	72.66	86.49	89.91	85.31	72.06	72.34	71.94
CaN	88.39	85.63	88.33	88.00	85.75	83.76	78.89
Norms							
Oliv	44.04	44.08	44.14	39.64	35.34	33.72	28.94
Plag	53.22	50.15	51.56	47.28	38.26	39.1	33.96
Cpx	–	–	–	3.41	20.23	21.17	26.54
Q	–	4.9	1.29	9.24	4.41	4.13	8.56
Ilm	0.09	0.11	0.11	0.19	0.65	0.77	1.89
Crt	0.46	0.03	0.03	0.23	1.11	1.11	0.08
Ap	0.02	0.06	–	0.01	–	–	0.03
Cor	0.05	0.65	2.86	–	–	–	–
Per	2.13	–	–	–	–	–	–
ppm							
Sr	82	104	98	103	118	120	79.6
Y	1.57	0.86	0.68	0.39	15.1	17.3	20.2
Zr	0.90	1.49	0.55	0.85	5.41	6.69	27.2
La	0.04	0.14	0.11	0.07	0.16	0.21	1.18
Nd	0.22	0.48	0.28	0.16	0.83	1.01	3.68
Sm	0.09	0.22	0.09	0.05	0.41	0.62	1.60
Eu	0.14	0.19	0.19	0.08	0.34	0.33	0.684
Yb	0.28	0.07	0.07	0.05	1.89	2.02	2.11

What has been trapped?

Olivine phenocryst S2-OL54 may have trapped a tiny piece of a troctolite. However, this seems unlikely as the small size of the inclusion (60 μm) would suggest an unrealistically fine-grained texture of the troctolite.

Instead, we suggest that the host olivine trapped a small crystal of plagioclase. The high temperature of magma at the moment of olivine crystallisation (~1,275 °C, see above) caused the plagioclase to react with its host, forming melt and residual high-Al spinel (the olivine component in the bulk inclusion composition in this scenario is 'supplied' by the host olivine). Thus, the observed phase composition of the inclusion (melt and spinel) is a function of the temperature of the host magma. If plagioclase were trapped by an olivine

growing from a cooler, more evolved, plagioclase-saturated (i.e. olivine–plagioclase cotectic) magma, the included plagioclase would not have melted and would remain as a solid inclusion. Such inclusions are quite common in MORB olivine phenocrysts (Sobolev et al. 1989; McNeill 1997; Kamenetsky, personal communication; Danyushevsky, unpublished data). On the other hand, if the host magma temperature was significantly higher, a larger amount of the host olivine would melt when reacting with the host plagioclase, leading eventually to the dissolution of the spinel inside the inclusion.

This origin of the inclusion is consistent with its low S, Cr_2O_3 and TiO_2 contents. The very low TiO_2 content of the inclusion also suggests that the amount of basaltic melt trapped together with plagioclase was negligible, if any.

The inclusion composition also reflects its partial equilibration with Fo_{90} (host olivine). The fact that equilibration occurred is demonstrated by the diffusion profiles of Ca and Cr in olivine around the inclusion (Fig. 4c). Diffusion of Ca from the inclusion is caused by the fact that the melt inside the inclusion has too high a CaO content to be in equilibrium with the olivine host. The amount of Ca that diffused out of the inclusion (~0.15 wt% CaO; estimated assuming inclusion and olivine densities of 2.65 and 3.3 g/cm^3, respectively, and the length of the diffusion profile in olivine of 30 μm, Fig. 4c) is insignificant, being close to the accuracy of electron microprobe analysis. At the same time, the amount of Cr_2O_3 gained (~0.1 wt%) is significant as it represents almost a third of the total Cr content of the inclusion.

Fe and Mg must have been also exchanged between the inclusion and the host, as their proportion in the inclusion is different from that in the melted olivine. The lack of detectable Fe and Mg diffusion profiles around the inclusion (Fig. 4c, MgO not shown) thus indicates that their contents in the inclusion have equilibrated nearly completely. Complete equilibration of Fe and Mg and partial equilibration of Ca and Cr are consistent with Fe–Mg inter-diffusion in olivine being significantly faster than tracer diffusion of Ca, and particularly Cr (e.g. Chakraborty 1997). Using the diffusion model of Danyushevsky et al. (2002), the time required for complete Fe–Mg equilibration is estimated to be ~1.5 months at 1,275 °C (temperature of trapping). Note that if the inclusion re-equilibrated with the olivine host at temperatures significantly below trapping (> 25 °C), it would have had a lower FeO* content than in other inclusions from this sample (see Danyushevsky et al. 2000), which is not observed (Fig. 2b).

Origin of the trapped plagioclase

As olivine phenocrysts crystallised from a hot strongly plagioclase-undersaturated magma, the plagioclase trapped by olivine S2-OL54 was a xenocryst. We suggest that it originated from a partially crystallised portion of the magma chamber. As plagioclase-saturated magmas have recently erupted within the transform (Fig. 2a), a plagioclase-bearing mush zone should exist within the transform crust. A hot primitive magma is expected to interact with a pre-existing colder mush zone. This interaction will involve, on the one hand, localised rapid cooling of the primitive magma, which should facilitate trapping of inclusions by the growing olivine phenocrysts and, on the other hand, dissolution of the minerals in the mush zone and its partial mixing with the primitive magma. The small size of the trapped plagioclase (~60 μm) could be a result of its partial dissolution prior to entrapment.

The composition of the trapped plagioclase (Ca# of the bulk inclusion composition, Table 4) is $\sim An_{88}$. It is within the high-An group of plagioclase present in the sample (see above), which may suggest that this population of plagioclase is also xenocrystic and represents disintegrated remnants of the assimilated mush zone.

Alternatively, plagioclase could originate from a disintegrated larger piece of a solid gabbroic/troctolitic wall rock of the conduit used by the ascending primitive magma. Small millimetre-sized xenoliths that range in composition from troctolites to olivine gabbros have been observed in more evolved plagioclase + olivine phyric lavas recovered from this area; however, these can also be parts of an assimilated mush zone. Similar gabbroic xenoliths described in lavas erupted at the EPR axis close to the Siqueiros transform (Ridley et al. 2001) and at the Gorda Ridge (Davis and Clague 1990) have also been interpreted as parts of a mush zone in a sub-axial magma chamber.

To summarise, the importance of this unusual inclusion is that (1) it demonstrates assimilation of plagioclase-rich material by primitive plagioclase-undersaturated Siqueiros magmas, and (2) it helps to understand the origin of 'intermediate' inclusions in phenocryst S1-OL24 which, as we discuss below, are quite common in high-Fo olivine phenocrysts in MORB.

Origin of melt inclusions in olivine phenocryst S1-OL24

Many compositional features of glasses and spinels from inclusions 2 and 3 from this grain (Figs. 1d, 3, 5, 6, Tables 1, 2, 3) are intermediate between 'normal' inclusions and the inclusion in olivine S2-OL54 described above. As in inclusion S2-OL54, similar compositional features of the melt and spinel in these inclusions (low Ti and high Al contents) suggest that the two phases are likely to be cogenetic. However, despite the general intermediate character of these inclusions, there are clear exceptions. The CaO and Sr contents in them are higher than in both 'normal' inclusions and inclusion S2-OL54, whereas the heavy REE are the same as in the 'normal' inclusions.

Melt inclusions similar to inclusions 2 and 3 in this phenocryst have been described in Siqueiros picrites by Sobolev et al. (1992), who suggested that their depletion

in incompatible elements (UDM signature) reflects melting processes in the ascending mantle beneath the ridge. Further, they suggest that these inclusions are samples of independently crystallising melt fractions separated from the top of the mantle melting column, which represent the highest degrees of mantle melting in this area. However, this explanation is inconsistent with higher Al_2O_3 and lower Cr_2O_3 contents of the melt, and lower Cr# of associated spinel, compared with 'normal' inclusions because these compositional features are opposite to what is expected for higher degree partial melts. Furthermore, Sobolev et al. (1992) do not take into account the lack of equilibrium between the initial composition of the trapped inclusion and the host phenocryst, exemplified by the diffusion profiles of Cr and Ca around the inclusions (Fig. 4d). This indicates that, similar to inclusion S2-OL54, inclusions 2 and 3 do not represent the melt from which the phenocryst grew. This melt is represented by the composition of 'normal' inclusion 1 (Fig. 1d, Tables 1, 3) which is similar to the host lava.

The bulk composition of inclusions 2 and 3 (glass, corrected for olivine fractionation on the walls, plus spinel) is presented in Table 4, nos. 5 and 6 (see above for calculation details). Unlike the inclusion in S2-OL54, the bulk composition of these inclusions cannot represent the unmodified composition of a contaminant. One manifestation of partial mixing with the host magma prior to entrapment is higher Cr_2O_3 contents of spinel and melt, resulting in bulk Cr_2O_3 contents of ~0.8 wt%, which is too high for plagioclase-rich assemblages alone. This can be demonstrated by assuming that the normative composition of these inclusions (Table 4) is representative of the modal composition of their source. Assuming 1.4 wt% Cr_2O_3 in clinopyroxene and 0.1 wt% in olivine, which are the maximum Cr_2O_3 contents in these minerals in MORB (see Appendix in Danyushevsky 2001), the bulk Cr_2O_3 contents in these inclusions are <0.35 wt%. Similar Cr_2O_3 contents are typical for plagioclase-rich lithologies in the oceanic crust (<0.3 wt%; e.g. Casey Benoit et al. 1996; 1997; Dick et al. 2000; Falloon, unpublished data). Note also that this high Cr_2O_3 content cannot result from Cr diffusion into the inclusion after trapping because the diffusion profiles around these inclusions are less pronounced than around the inclusion in S2-OL54 (cf., Fig. 4c, d), and thus the amount of Cr_2O_3 gained by the inclusions is <0.1 wt% (see above).

We suggest two possibilities for the origin of these inclusions. In both cases these inclusions represent localised dissolution of earlier formed gabbroic 'cumulates' within the mush zone while the hot primitive magma was passing through, but unlike inclusion S2-OL54, they also reflect partial assimilation of the dissolution products into the primitive magma prior to entrapment. In both cases the degree of mixing was not large.

One possibility is that olivine S1-OL24 trapped the reaction products of plagioclase with the host magma. As discussed by Bedard (1993) and Bedard and Hebert (1998), plagioclase incorporated into a hot, plagioclase under-saturated primitive basaltic magma will melt incongruently, producing high-Al spinel. The melt produced by the reacting plagioclase will mix with the host magma. This mixing on such a fine scale should be primarily controlled by diffusion rates of elements in both melts and, thus, variations in the degree of equilibration can be expected for different elements. The presence of spinel in both inclusions is a further indication that entrapment occurred quickly after assimilation began, otherwise spinel would separate from the assimilating melt (being significantly denser) and react with the host magma, increasing spinel's Cr content. A potential problem with this mechanism is that it is difficult to reconcile the high CaO/Na_2O and Sr content of the bulk composition. The 100*Ca/(Ca + Na) (Ca#) value of the partially mixed trapped compositions (~85, Table 4) suggests that the assimilated plagioclase was similar in composition to plagioclase trapped by phenocryst S2-OL54. Thus, it is difficult to explain why partially mixed inclusions have significantly higher Sr contents (but smaller Sr anomalies) than the 'pure' plagioclase inclusion in S2-OL54.

A more likely scenario is the simultaneous dissolution of plagioclase and a subordinate amount of clinopyroxene. Assimilation of such assemblages by a primitive basaltic magma should also produce a residual spinel (Presnall et al. 1978; Onuma and Tohara 1983;Bedard et al. 2000). The presence of clinopyroxene in the contaminant can explain high CaO contents of the inclusions and the overall higher concentrations of all incompatible elements, and especially of middle and heavy REE, which are more compatible in clinopyroxene (e.g. Blundy et al. 1998, and references therein). Moreover, if the assimilation mechanism involved diffusion, then smaller differences in heavy REE contents between the contaminant and the host magma may disappear faster than larger differences in more incompatible elements. This can explain the similarities in heavy REE contents in inclusions 2 and 3, compared with the 'normal' inclusions. Smaller proportions of plagioclase in the contaminant are consistent with the smaller observed Sr, Eu and Zr anomalies (Fig. 5a). The low-An plagioclase xenocrysts present in the sample (see above) may represent disseminated fragments of this gabbroic material. A higher Sr content expected for the low-An plagioclase compared with high-An plagioclase could also explain the higher Sr content of the inclusion.

Unlike inclusion S2-OL54, inclusions in olivine S1-OL24 do not have elevated Cl contents. Different compositions of plagioclase in the contaminants trapped by these two olivines may suggest that assimilation occurred at different levels of the magmatic system (e.g. different parts of the mush zone). Higher Cl contents in inclusion S2-OL52 may then indicate that, unlike the low-An contaminant, the high-An contaminant has interacted with hydrothermal fluids prior to reaction with the primitive magma. High Cl contents observed in plagioclase-hosted ultra-depleted melt inclusions with negative Zr anomalies from a number of MORB

samples (Nielsen et al. 2000) may reflect a similar assimilation processes to that proposed here.

Alternative explanations for the origin of anomalous inclusions

It is theoretically possible that olivine grain S2-OL54 originally had a more evolved (lower Fo) composition and crystallised from a more evolved, olivine–plagioclase cotectic melt. As discussed above, such olivine phenocrysts often contain small inclusions of plagioclase. If such a grain was picked up by a hot primitive magma, the plagioclase inclusion will melt, producing residual high-Al spinel, and if there is sufficient time for this grain to equilibrate with the host magma completely, its compositions will not differ from other olivine phenocrysts in the rock. In this case the inclusion in grain S2-OL54 is not a result of assimilation of plagioclase.

Sobolev et al. (2000) have suggested that inclusions similar to 2 and 3 in olivine S1-OL24 represent melt fractions originated from mantle heterogeneities caused by the reaction of recycled crustal gabbro with mantle peridotites. At pressures less than 10 kbar such heterogeneities may contain plagioclase, and if melting under the Siqueiros Transform occurred at low pressures, melt fractions from these heterogeneities may have compositions similar to those of inclusions 2 and 3 in olivine S1-OL24. Saal et al. (2001), on the other hand, have suggested that such inclusions represent melts originated from depleted lithospheric harzburgite impregnated by gabbroic dykes, which has been re-melted under the transform fault during an extension event.

A detailed analysis of these hypotheses is beyond the scope of this paper. However, we note that accepting any one of them demands that the origins of inclusion S2-OL54 and inclusions 2 and 3 in S1-OL24 must be unrelated. Given the obvious similarity in compositional features of these inclusions and the overall rarity of such inclusions in MORB olivine phenocrysts, we do not believe that their coexistence in a single sample is a mere coincidence. Furthermore, there is mineralogic evidence for assimilation of plagioclase-rich assemblages in Siqueiros basalts and picrites (low-An plagioclase xenocrysts and gabbroic clots, see above).

Comparison with anomalous melt inclusions from other localities

Melt inclusions with large positive Sr anomalies and incompatible element contents lower than in their host lavas and/or melt inclusions without Sr anomalies have also been reported in olivine phenocrysts from Iceland, and the MAR (Fig. 7b, c). Similar to inclusions 2 and 3 from olivine S1-OL24 (Fig. 7a), they all have heavy REE contents comparable with those in 'normal' inclusions, and also have positive Eu and negative Zr anomalies. Spinel associated with the anomalous MAR inclusions has higher Al_2O_3 content than other spinel in this sample (Kamenetsky et al. 1998). We suggest that the compositions of all these inclusions reflect a similar assimilation process to that proposed here. The contents of highly incompatible elements in such inclusions (UDM-like from Siqueiros and Iceland; more 'normal' from northern MAR) reflect (1) their concentrations in the host magma, (2) the degree of mixing between the melted contaminant and the host melt prior to entrapment, and (3) the composition of the contaminant. The extent of the positive Sr and Eu anomalies also depends on the amount and composition of plagioclase in the contaminant. It appears that clinopyroxene-bearing assemblages have been assimilated in these other localities because inclusions have high CaO contents and contain significant abundances of heavy REE and Ti. The assimilation of pure plagioclase should result in inclusions having significantly lower contents of heavy REE (e.g. inclusion in olivine S2-OL54, Fig. 5a; see discussion above).

Similarly to the anomalous Siqueiros inclusions, inclusions from Iceland also have higher Al_2O_3 contents, whereas MAR inclusions with positive Sr anomalies have Al_2O_3 contents similar to 'normal' inclusions. The Al_2O_3 content of a melt in equilibrium with olivine and aluminous spinel is a function of the Cr_2O_3 content of the system (Al_2O_3 in the melt decreases with increasing Cr_2O_3; Onuma and Tohara 1983). Mixing of the contaminant with the host magma while it dissolves prior to entrapment, leads to an increase of the Cr_2O_3 content of both the residual spinel and melt and, thus, to a decrease of the melt Al_2O_3 content (the excess Al_2O_3 is accommodated in the spinel). As can be seen on Fig. 7, the MAR inclusion has the highest contents of highly incompatible elements and, thus, possibly reflects a higher degree of mixing with the host magma, which can explain its 'normal' Al_2O_3 content.

Gurenko and Chaussidon (1995) and Kamenetsky et al. (1998) suggested that Sr anomalies in inclusions from Iceland and northern MAR result from melting of plagioclase-bearing peridotitic mantle. However, even if melting in these two regions occurred within the plagioclase stability field, plagioclase is exhausted from the MORB mantle source at $< \sim 4\%$ melting (Falloon et al. 1999; Falloon et al., unpublished), whereas major element compositions of all these melts are consistent with much larger degrees of melting. For example, mantle melts in equilibrium with plagioclase lherzolite have low CaO (< 10 wt%) and high Na_2O (> 3.5 wt%) contents, whereas these melt inclusions have high CaO (> 13 wt%) and low Na_2O (< 2 wt%) concentrations.

UDM inclusions in olivine from MORB recovered around 9°N on the MAR (Sobolev and Shimizu 1993; Fig. 7d) are quite different from the inclusions described above. They do not have Sr, Eu and Zr anomalies, and their heavy REE concentrations are significantly lower than in the associated glasses (Fig. 7d). Such compositions are more consistent with high degrees of mantle melting at depths above garnet stability field, or melting of an incompatible element-depleted mantle source.

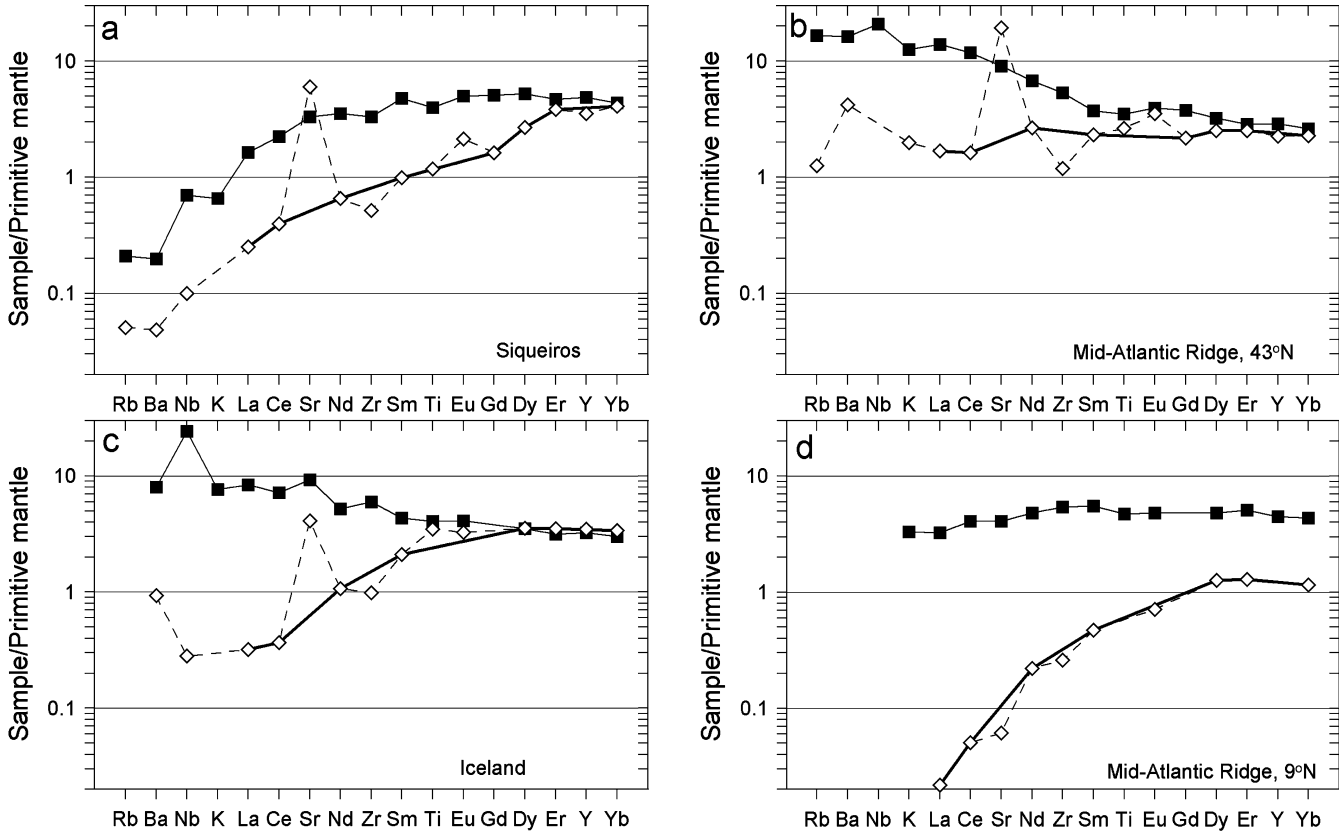

Fig. 7a–d UDM and/or Sr-enriched melt inclusions in primitive olivine phenocrysts from MORB from different localities. *Open diamonds* Anomalous melt inclusions; *solid squares* 'normal', i.e. not anomalous, melt inclusions from the same samples or pillow-rim glass of the sample; *thick solid line* connects REE of anomalous inclusions, excluding Eu, and is used to highlight Sr, Zr and Eu anomalies in these inclusions. **a** Inclusions from Siqueiros FZ, this study; **b** inclusions from 43°N MAR, Kamenetsky et al. (1998); **c** inclusions from Iceland, Gurenko and Chaussidon (1995); **d** UDM inclusion from 9°N MAR and pillow-rim glass Sobolev and Shimizu (1993). See text for discussion

'Normal' melt inclusions from sample ALV-2384-3

Although compositions of 'normal' inclusions are generally consistent with being representative of parental melts for the pillow-rim glasses (Figs. 3, 5), some clear differences exist. In particular, 'normal' melt inclusions have higher Al_2O_3 and CaO, and lower TiO_2 and Na_2O contents, resulting in higher CaO/Na_2O values than in the calculated parental melt (Fig. 3). All these features are pronounced in the compositions of the two contaminants described in the previous sections and, thus, it appears the compositions of 'normal' melt inclusions are also affected (but to a significantly lesser degree) by a similar assimilation processes.

Correlations between the size of Sr anomaly and CaO/Na_2O values is observed in only a few 'normal' melt inclusions (Fig. 8a), one of which is inclusion 1 from grain S1-OL24 that also hosts two anomalous inclusions. The lack of Sr anomalies in other 'normal' melt inclusions may reflect a different composition of the contaminant, perhaps dominated by clinopyroxene.

The most intriguing feature of 'normal' melt inclusions is a positive correlation between their CaO/Na_2O values and La and Ce contents (Fig. 8b, c). This correlation cannot be due to assimilation of mineral phases in the mush zones as all of them have lower concentrations of incompatible elements than the melt. However, assimilation of crystals together with small amounts of the residual inter-cumulus melts from the mush zone may produce the observed trends, as such melts are expected to be enriched in incompatible elements. A similar process can explain the coupled Sr anomaly and high incompatible element contents in inclusion S1-OL59 (Fig. 5b).

In general, we suggest that the type of assimilation we discuss in this paper occurs on a very small scale when the primitive melts are interacting with crystals and possibly residual melts in a pre-existing mush zone. In such an environment the contaminants are expected to have quite diverse compositions, which is reflected in the variety of compositions of anomalous and 'normal' melt inclusions.

Implications for studies of MORB petrogenesis

The type of assimilation we discuss should have the largest impact on the compositions of melt inclusions trapped by phenocrysts crystallising from hot primitive magmas (mainly high-Fo olivine, but also spinel and in some cases plagioclase). Interaction of such magmas with cooler crustal mush zones and/or wall-rocks will

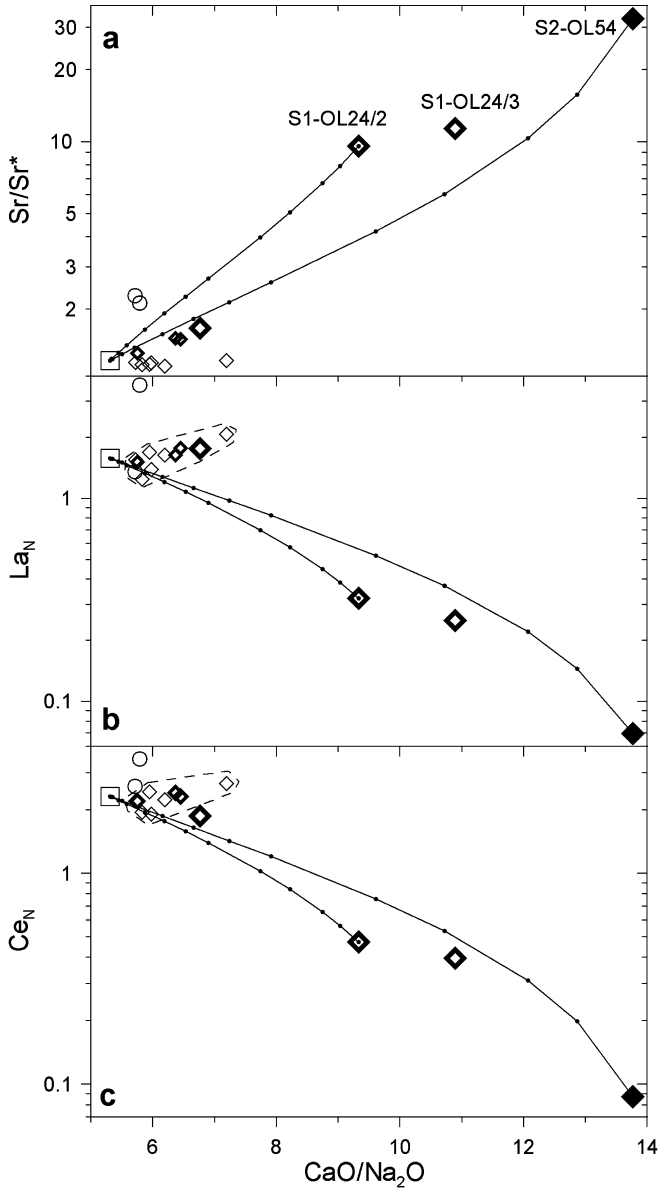

Fig. 8 Compositional variations in 'normal' melt inclusions from sample ALV-2384-3. *Symbols* as on Fig. 2. *Dashed lines* outline 'normal' melt inclusions. *Solid lines with small dots* are mixing trends of melt inclusion compositions S2-OL54 and S1-OL24/2 with the composition of the pillow-rim glass of this sample. The composition of the pillow-rim glass was corrected for olivine fractionation to have 12 wt% MgO (Fig. 3). Three 'normal' melt inclusions with elevated Sr anomalies are shown by *small bold diamonds*. No anomalous inclusions have been found in the grains hosting these three inclusions. See text for discussion

cause localised rapid cooling, facilitating crystallisation at the margins of the magma and also trapping of inclusions by the growing phenocrysts. The compositions of these melt inclusions are likely to record the processes of partial dissolution of the crustal material and its mixing with the primitive magma. Thus, the observed variability in melt inclusion compositions in primitive MORB phenocrysts need not always reflect processes occurring in the mantle (see a detail discussion in Bedard et al. 2000). In particular, inferences on fractional melting processes based on geochemistry of ultra-depleted melt inclusions may not always be valid.

For example, Sobolev and Hofmann (1999) have interpreted low S contents in depleted Siqueiros melt inclusions (similar to those in phenocryst S1-OL24) to indicate S-undersaturation of high-degree melts from MORB mantle source. However, these Siqueiros inclusions cannot be used to infer primary magma generation parameters and their low S contents are a reflection of the low S contents in the contaminants. Another example is 'normal' inclusions in Siqueiros olivines. Even if one rejects our arguments that their compositions are also affected by assimilation, the positive correlation between La, Ce and CaO/Na_2O values (Fig. 8b, c) rules out variations in the degree of melting as the cause of the observed compositional variations since the smaller degrees of melting required to enrich La would also enrich Na and decrease Ca, resulting in lower CaO/Na_2O values.

At the same time, the assimilation process we discuss appears to have little effect on the compositions of erupted MORB, which is supported by the lack of an assimilation signature in pillow-rim glass and whole-rock compositions of the Siqueiros picrites. However, the important aspect of the results, also supported by studies of gabbroic xenoliths in MORB (Davis and Clague 1990; Ridley et al. 2001) and studies of ophiolites (Bedard 1993; Bedard and Hebert 1998; Bedard et al. 2000), is that primitive melts interact with gabbroic material en route to the surface, and this interaction should be accounted for in models for the generation of typical MORB lavas. Consistent with our results, the most noticeable effect of primitive melt reaction with the material represented by gabbroic xenoliths is plagioclase dissolution (Ridley et al. 2001)

Acknowledgements This research was supported by the Australian Research Council through QEII Research Fellowship and Research Grants to LVD and by the National Science Foundation under grant OCE-90-19154 to MRP. We wish to thank Dan Fornari for his expertise during the original field program and his continued support of the geochemical research. Stimulating discussions with Dima Kamenetsky, Alex Sobolev, Ilia Veksler and Tony Crawford have clarified many initial ideas and interpretations. The paper has benefited from the formal review by an anonymous reviewer and from comments by A. Sobolev, C. Ballhaus and D. Ionov. We acknowledge support of the Museum of Natural History, Washington, DC, which provided electron microprobe standards.

References

Bedard JH (1993) Oceanic crust as a reactive filter: synkinematic intrusion, hybridization, and assimilation in an ophiolitic magma chamber, western Newfoundland. Geology 21:77–80

Bedard JH, Hebert R (1998) Formation of chromitites by assimilation of crustal pyroxenites and gabbros into peridotitic intrusions: North Arm Mountain Massif, Bay of Islands ophiolite, Newfoundland, Canada. J Geophys Res 103:5165–5184

Bedard JH, Hebert R, Berclaz A, Varfalvy V (2000) Syntexis and the genesis of lower oceanic crust. Geol Soc Am Spec Pap 349:105–119

Benoit M, Polve M, Ceuleneer G (1996) Trace element and isotopic characterisation of mafic cumulates in a fossil diapir (Oman ophiolite). Chem Geol 134:199–214

Bindeman IN, Davis AM (2000) Trace element partitioning between plagioclase and melt: Investigation of dopant influence on partition behavior. Geochem Cosmochim Acta 64:2863–2878

Blundy JD, Robinson JAC, Wood BJ (1998) Heavy REE are compatible in clinopyroxene on the spinel lherzolite solidus. Earth Planet Sci Lett 160:493–504

Casey JF (1997) Comparison of major- and trace-element geochemistry of abyssal peridotites and mafic plutonic rocks with basalts from the MARK region of the Mid-Atlantic Ridge. In: Karson JA, Cannat M, Miller DJ, Elthon D (eds.) Proc ODP Sci Results 153, College Station, TX (ODP), pp 181–241

Chakraborty S (1997) Rates and mechanisms of Fe–Mg interdiffusion in olivine at 980°–1,300°C. J Geophys Res 102B:12317–12331

Constantin M (1999) Gabbroic intrusions and magnetic metasomatism in harzburgites from the Garrett transform fault: implications for the nature of the mantle-crust transition at fast-spreading ridges. Contrib Mineral Petrol 136:111–130

Danyushevsky LV (2001) The effect of small amounts of H_2O on crystallisation of mid-ocean ridge and backarc basin magmas. J Volcanol Geotherm Res 110:265–280

Danyushevsky LV, Sobolev AV (1996) Ferric–ferrous ratio and oxygen fugacity calculations for primitive mantle-derived melts: calibration of an empirical technique. Mineral Petrol 57:229–241

Danyushevsky LV, Sobolev AV, Dmitriev LV (1988) Orthopyroxene-bearing low-Ti tholeiites as a new type of mid-ocean ridge tholeiites Trans USSR Acad Sci Earth Sci 292:102–105

Danyushevsky LV, Della-Pasqua, FN, Sokolov S (2000) Re-equilibration of melt inclusions trapped by magnesian olivine phenocrysts from subduction-related magmas: petrological implications. Contrib Mineral Petrol 138:68–83

Danyushevsky LV, Sokolov S, Falloon TJ (2002) Melt inclusions in olivine phenocrysts: using diffusive re-equilibration to determine the cooling history of a crystal, with implications for the origin of olivine-phyric rocks. J Petrol 43(9):1651–1671

Davis AS, Clague DA (1990) Gabbroic xenoliths from the northern Gorda Ridge: implications for magma chamber processes under slow spreading ridges. J Geophys Res 95B:10885–10905

Della-Pasqua FN, Kamenetsky VS, Gasparon M, Crawford AJ, Varne R (1995) Al-spinels in primitive arc volcanics. Mineral Petrol 53:1–26

Dick HJB, Natland JH (1996) Late-stage melt evolution and transport in the shallow mantle beneath the East Pacific Rise. In: Mevel C, Gilis KM, Allan JF, Meyer PS (eds) Proc ODP Sci Results 147, College Station, TX (ODP), pp 103–134

Dick HJB, Natland JH, Leg 176 Scientific Party (2000) A long in situ section of the lower oceanic crust: results of ODP Leg 176 drilling at the Southwest Indian Ridge. Earth Planet Sci Lett 179:31–51

Eggins SM, Kinsley LPJ, Shelley JMG (1998a) Deposition and element fractionation processes during atmospheric pressure laser sampling for analysis by ICPMS. Appl Surface Sci 127–129:278–286

Eggins SM, Rudnick RL, McDonough WF (1998b) The composition of peridotites and their minerals: a laser-ablation ICP-MS study. Earth Planet Sci Lett 154:53–71

Elthon D, Karson JA, Casey JF, Sullivan J, Siroky FX (1986) Geochemistry of diabase dikes from the Lewis Hills Massif, Bay of Islands ophiolite: evidence for partial melting of oceanic crust in transform faults. Earth Planet Sci Lett 78:89–103

Falloon TJ, Green DH, Danyushevsky LV, Faul UH (1999) Peridotite melting at 1.0 and 1.5 GPa: an experimental evaluation of techniques using diamond aggregates and mineral mixes for determination of near-solidus melts. J Petrol 40:1343–1375

Ford CE, Russel DG, Craven JA, Fisk MR (1983) Olivine–liquid equilibria: temperature, pressure and composition dependence of the crystal/liquid cation partition coefficients for Mg, Fe^{2+}, Ca and Mn. J Petrol 24:256–265

Garrido CJ, Bodinier J-L, Alard O (2000) Incompatible trace element partitioning and residence in anhydrous peridotites and websterites from the Ronda orogenic peridotite. Earth Planet Sci Lett 181:341–358

Green TH (1994) Experimental studies of trace-element partitioning applicable to igneous petrogenesis – Sedona 16 years later. Chem Geol 117:1–36

Gurenko AA, Chaussidon M (1995) Enriched and depleted primitive melts included in olivine from Icelandic tholeiites – origin by continuous melting of a single mantle column. Geochim Cosmochim Acta 59:2905–2917

Hemond C, Arndt NT, Lichtenstein U, Hofmann AW (1993) The heterogeneous Iceland Plume: Nd–Sr–O isotopes and trace element constraints. J Geophys Res 98B:15833–15850

Horn I, Foley SF, Jackson SE, Jenner GA (1994) Experimentally determined partitioning of high field strength and selected transition elements between spinel and basaltic melt. Chem Geol 117:193–218

Jarosewich EJ, Nelen JA, Norberg JA (1980) Reference samples for electron microprobe analyses. Geostand Newsl 4:257–58

Kamenetsky VS (1996) Methodology for the study of melt inclusions in Cr-spinel, and implications for parental melts of MORB from FAMOUS area. Earth Planet Sci Lett 142:479–486

Kamenetsky VS, Eggins SM, Crawford AJ, Green DH, Gasparon M, Falloon TJ (1998) Calcic melt inclusions in primitive olivine at 43°N MAR: evidence for melt-rock reaction/melting involving clinopyroxene-rich lithologies during MORB generation. Earth Planet Sci Lett 160:115–132

Longerich HP, Jackson SE, Gunther D (1996) Laser ablation inductively coupled plasma mass spectrometric transient signal data acquisition and analyt concentration calculation. J Anal Atomic Spectrom 11:899–904

Maurel C, Maurel P (1982) Etude experimentale de l'equilibre Fe^{2+}-Fe^{3+} dans les spinelles chromiferes et les liquides silicates basiques coexistants, a 1 atm. C R Acad Sci Paris 285: 209–215

McNeill AW (1997) The crystallisation history of normal mid-ocean ridge basalts from the eastern Pacific Ocean and implications for the composition of primary mid-ocean ridge magmas: evidence from mineralogy, pillow-rim glasses and melt inclusion studies. PhD Thesis, University of Tasmania, Hobart

Nielsen RL, Sours-Page RE, Harpp KS (2000) Role of a Cl-bearing flux in the origin of depleted ocean floor magmas. Geochem Geophys Geosys 1:17

Onuma K, Tohara T (1983) Effect of chromium on phase relations in the join forsterite–anorthite–diopside in air at 1 atm. Contrib Mineral Petrol 84:174–181

Perfit MR Fornari DJ, Ridley WI, Kirk PD, Casey J, Kastens KA, Reynolds JR, Edwards M, Desonie D, Shuster R, Paradis S (1996) Recent volcanism in the Siqueiros transform fault: picritic basalts and implication for MORB magma genesis. Earth Planet Sci Lett 141:91–108

Pockalny RA, Fox PJ, Fornari DJ, Macdonald KC, Perfit MR (1997) Tectonic reconstruction of the Clipperton and Siqueiros Fracture Zones: evidence and consequences of plate motion change for the last 3 Myr. J Geophys Res 102B:3167–3181

Presnall DC, Dixon SA, Dixon JR, O'Donnell TH, Brenner NL, Schrock RL, Dycus DW (1978) Liquidus phase relations on the join diopside–forsterite–anorthite from 1 atm to 20 kbar: their bearing on the generation and crystallisation of basaltic magmas. Contrib Mineral Petrol 66:203–220

Ridley WI, Perfit MR, Smith MC (2001) On magmatic processes at fast-spreading ridges as revealed in a xenolith from the mush zone beneath the East Pacific rise at 9°50′N. EUG XI Abstr 307

Saal AE, Hauri E, Langmuir CH, Perfit M (2001) Undersaturated volatile contents in MORB, evidence for re-melting episodes. Eos 82, AGU Fall Meeting Suppl F1401

Sobolev AV, Hofmann AW (1999) Incompatible behavior of Sulfur in ultra-depleted MORB. Ofioliti 24:166

Sobolev AV, Shimizu N (1993) Ultra-depleted primary melt included in an olivine from the Mid-Atlantic Ridge. Nature 363:151–154

Sobolev AV, Danyushevsky LV, Dmitriev LV, Suschevskaya NM (1989) High-alumina magnesian tholeiite as the primary basalt magma at Midocean ridge. Geochem Int 26(5):128–133

Sobolev AV, Casey JF, Shimizu N, Perfit M (1992) Contamination and mixing of MORB primary melts: evidence from inclusions study in Siqueiros picrites. EOS 73, AGU Spring Meeting Suppl 336

Sobolev AV, Gurenko AA, Shimizu N (1994) Ultra-depleted melts from Iceland: data from melt inclusion studies. Mineral Mag 58A:860–861

Sobolev AV, Hofmann AW, Nikogosian IK (2000) Recycled oceanic crust observed in 'ghost plagioclase' within the source of Mauna Loa lavas. Nature 404:986–990

Sun S-S, McDonough WF (1989) Chemical and isotopic systematics of oceanic basalts: implication for mantle composition and processes. In: Saunders AD, Norry MJ (eds) Magmatism in the ocean basins. Geol Soc Spec Publ 42:313–45